Global and Planetary Change 172 (2019) 374–395

Contents lists available at ScienceDirect

Global and Planetary Change

journal homepage: www.elsevier.com/locate/gloplacha

Research article

Integrated bio-magnetostratigraphy of the Badenian reference section Ugljevik in southern Pannonian Basin - implications for the Paratethys history (middle Miocene, Central Europe)

Oleg Mandic[a,*], Karin Sant[b], Mădălina-Elena Kallanxhi[c], Stjepan Ćorić[d], Dörte Theobalt[a], Patrick Grunert[e], Arjan de Leeuw[f], Wout Krijgsman[b]

[a] Geological-Paleontological Department, Natural History Museum, Burgring 7, 1010 Vienna, Austria
[b] Paleomagnetic Laboratory Fort Hoofddijk, Department of Earth Sciences, Utrecht University, Budapestlaan 17, 3584 CD Utrecht, the Netherlands
[c] Department of Geology, Faculty of Biology and Geology, Babeş-Bolyai University, M. Kogălniceanu 1, 400084 Cluj-Napoca, Romania
[d] Geological Survey of Austria, Neulinggasse 38, 1030 Vienna, Austria
[e] Institute of Geology and Mineralogy, Faculty of Mathematics and Natural Sciences, University of Cologne, Zülpicher Str. 49a, 50674 Köln, Germany
[f] Univ. Grenoble Alpes, Univ. Savoie Mont Blanc, CNRS, IRD, IFSTTAR, ISTerre, 38000 Grenoble, France

ARTICLE INFO

Keywords:
Langhian
Serravallian
Paleoenvironment
Oxygen isotopes
Calcareous nannoplankton
Foraminifera
Mollusks

ABSTRACT

The Central Paratethys was a large-scale Oligo-Miocene epicontinental sea located in Central and Eastern Europe. It was separated from the Mediterranean by the Alpine orogenic belt. The Paratethys progressively flooded the Pannonian back-arc basin that formed during the early to middle Miocene. Along the southern margin of the basin, the maximum extension of the Paratethys onto the flanks of the Dinarides Mountains occurred during the middle Miocene (Badenian). We have studied the most complete middle Miocene (Badenian-Sarmatian) Paratethys section located at this southern margin. It comprises a > 1.5 Myr long, continuous marine depositional sequence, which is highly relevant for our understanding of the interplay between global climatic and regional geodynamic perturbations in this semi-isolated epicontinental basin. The investigated record is particularly important to assess the impact of the Middle Miocene Climate Transition, the Langhian-Serravallian glacial Mi-3b event, the *syn*-rift climax of the Pannonian Basin and the Badenian Salinity Crisis. Moreover, we present the first high resolution age model for the regional Badenian stage based on integrated biomagnetostratigraphy. According to our age model, the marine flooding reached the area at ~14.15 Ma, during the regional Badenian stage. Open marine conditions persisted until ~12.6 Ma when the extinction of the fully marine fauna marks the beginning of the regional Sarmatian stage. Sea-level fluctuations are reflected in the section by four transgressive regressive cycles coinciding roughly with 400-kyr-eccentricity periods. The largest sea-level fall occurred after the first cycle and corresponds to the end of the Middle Miocene Climate Transition marked by glacial event Mi-3b. Elsewhere in the Pannonian Basin, this marked drop in base-level triggered deposition of evaporites during the Badenian Salinity Crisis. At Ugljevik however, there are no evaporites and the short-term Mi-3b regression was followed by a transgression and re-establishment of deeper marine conditions at 13.76 Ma, i.e. during the earliest Serravallian. Diversified planktonic and benthic assemblages suggest fully marine conditions with a persistent connection to the Mediterranean at this time. Such conditions prevailed until the mid Serravallian (latest Badenian) when sediment input increased and coastal environments prograded seawards. The Badenian/Sarmatian boundary roughly coincided with a 400-kyr-eccentricity as well as with a 1.2-Myr obliquity minimum.

1. Introduction

The middle Miocene was a time of severe climatic change as a result of the Miocene Climatic Optimum (MCO, 16.8–14.7 Ma) and the Middle Miocene Climatic Transition (MMCT, 14.7–13.76 Ma) (Holbourn et al., 2007, 2014, 2015; Shevenell et al., 2004; Zachos et al., 2001, Fig. 1). The MCO represented a global warming phase crossing the Burdigalian/Langhian transition, while the MMCT involved the subsequent deterioration of Earth's climate in response to cooling of the deep oceans and Antarctic ice-sheet expansion (Holbourn et al., 2014). The end of

* Corresponding author.
E-mail address: oleg.mandic@nhm-wien.ac.at (O. Mandic).

https://doi.org/10.1016/j.gloplacha.2018.10.010
Received 13 August 2018; Received in revised form 4 October 2018; Accepted 19 October 2018
Available online 24 October 2018
0921-8181/

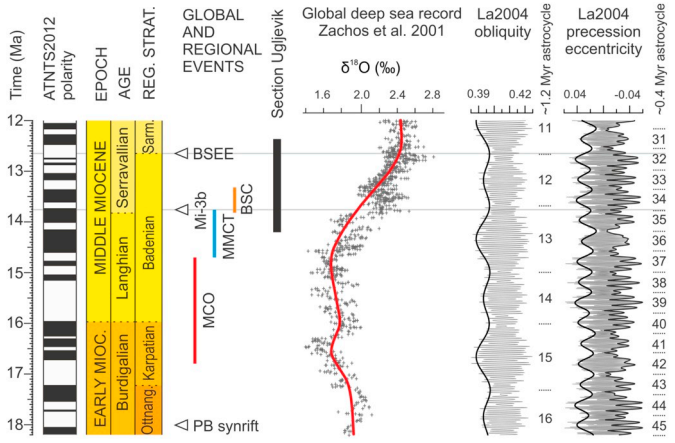

Fig. 1. Global and Mediterranean timescale after Hilgen et al. (2012) showing the main lower-middle Miocene events (PB = Pannonian Basin, MCO = Miocene Climatic Optimum, MMCT = Middle Miocene Climatic Transition, BSC = Badenian Salinity Crisis, BSEE = Badenian-Sarmatian Extinction Event), the age of the Ugljevik section, global $\delta^{18}O$ benthic foraminifera record (Zachos et al., 2001) and the orbital solution for the insolation quantities of the Earth (Laskar et al., 2004).

the MMCT is marked by a severe glacial, as indicated by a negative excursion in $\delta^{18}O$ at 13.76 Ma, accompanied by a glacio-eustatic sea-level drop of 59 ± 6 m (Mi-3b event) (John et al., 2011; Kominz et al., 2008). This event is recorded in numerous sedimentary archives around the globe, and defines the base of the Serravallian stage (Abels et al., 2005; Hilgen et al., 2012; 2009; Holbourn et al., 2014; Mourik et al., 2011).

The Central Paratethys was an ancient semi-isolated sea persisting in Central and Eastern Europe from the Oligocene to middle Miocene (Harzhauser and Piller, 2007; Popov et al., 2004; Rögl, 1998) (Fig. 2B). Its paleoenvironments and connecting sea-straits were largely determined by geodynamic, climatic and glacio-eustatic fluctuations (Kováč et al., 2017; Palcu et al., 2015; Sant et al., 2017). Their combined effects triggered the major southwards and eastwards expansion of the Central Paratethys in the middle Miocene, which is known as the Badenian marine flooding (Ćorić et al., 2009; Sant et al., 2017). During the Langhian to early Serravallian (regional Badenian stage), the sea was well-connected to the Mediterranean via the Slovenian gateway and covered most of the Pannonian Basin System and Carpathian Foredeep (Bartol, 2009; Bartol et al., 2014; Kováč et al., 2007, 2017) (Fig. 2B). The cooling-induced sea level drop at the Langhian/Serravallian transition was very pronounced in the eastern part of the Central Paratethys (Carpathian Foredeep and Transylvanian Basin), where massive evaporite packages were deposited during the so-called Badenian Salinity Crisis (BSC) (Bojar et al., 2018; de Leeuw et al., 2010; Peryt, 2006; Túnyi et al., 2005) (Fig. 1). Lasting for ~500 kyr, the BSC ended the latest at 13.32 ± 0.07 Ma (de Leeuw et al., 2018), thereafter, open marine conditions were re-established. Termination of open marine conditions in the late Serravallian subsequently triggered the Badenian/Sarmatian Extinction Event (BSEE), marked by the elimination of all stenohaline organisms in the Central and in the Eastern Paratethys (Harzhauser and Piller, 2004). Autochthonous speciation and radiation was followed by an increased faunal exchange resulting in unified Sarmatian endemic polyhaline assemblages throughout the Paratethys (Harzhauser and Piller, 2007; Palcu et al., 2015; Popov et al., 2004). A restricted connection with the Mediterranean remained active until the end of the Sarmatian and Serravallian, respectively (Bartol et al., 2014).

The Ugljevik section (Bosnia and Herzegovina) is located in the southernmost part of the Central Paratethys (Fig. 2A–B). The quarry section is unique, because it is the only continuous outcrop in the Central Paratethys that covers the Badenian marine flooding, the Mi-3b induced sea-level lowstand and the BSEE (Pezelj et al., 2013). Such a continuous succession was so far only available from a drill core (Báldi, 2006), thus providing an exceptional opportunity to study the paleoenvironmental changes during the Badenian in the southern part of the Central Paratethys Sea. We carried out an integrated stratigraphic and paleoenvironmental study including lithofacies, magnetostratigraphic, natural gamma ray, magnetic susceptibility, stable isotope, calcareous nannofossil, mollusk and foraminiferal analyses to produce a high-resolution age and depositional model for the Ugljevik section. The main paleoenvironmental changes are compared to regional Paratethys and global events.

2. Geological setting and regional geology

Ugljevik is located in the Sava depression at the southern margin of the Pannonian Basin (Fig. 2C–D). The underlying basement belongs to the Dinarides and includes the tectonic contact between the Jadar-Kopaonik thrust sheet and the Jurassic obducted Western Vardar Ophiolitic Unit (Schmid et al., 2008; Ustaszewski et al., 2008). The Jadar-Kopaonik terrane derives from the Adriatic passive margin and comprises a Paleozoic non-metamorphosed basement overlain by Permian to Triassic marine carbonates (Balázs et al., 2016; Tari and Pamić, 1998; Ustaszewski et al., 2014). Transgressive upper Cretaceous marine carbonates are in turn overlain by Paleocene to upper Eocene deposits composed of corallinacean limestones, shallow water sandstones with gastropods, paralic coal and flysch-like deposits (Čičić et al., 1991; 1990; Mojsilović et al., 1975; Malez and Thenius, 1985). The subsequent emersion of the northern Dinarides is reflected by Oligocene terrestrial and alluvial clays, sandstones and conglomerates (Fig. 2D). In the late Oligocene, lacustrine basins developed containing a coal succession with small and large mammal remains, followed by perennial lacustrine marl with numerous ostracods (de Leeuw et al., 2011; Hrvatović, 2006). At the Ugljevik locality, the continental basin infill ends with the late Oligocene coal-bearing series, separated from overlying middle Miocene marine Central Paratethys sediments by an angular unconformity (de Bruijn et al., 2013; Pezelj et al., 2013; Wessels et al., 2008).

The Sava depression formed as the result of back-arc extension of the Pannonian Basin that was active since ~18 Ma (Fodor et al., 1999; Horváth et al., 2015; Mandic et al., 2012; Lukacs et al., 2018), and most likely accelerated during middle Miocene times (Matenco and Radivojević, 2012; Stojadinović et al., 2013). The Miocene succession in Ugljevik begins with 137 m of marine deposits of the Badenian stage (Langhian-lower Serravallian) continuing with restricted marine deposits of the Sarmatian stage.

Pezelj et al. (2013) presented biostratigraphic and paleoenvironmental analyses based on calcareous nannoplankton and benthic foraminifera for the lowermost 63 m of the Ugljevik section (Fig. 3). Benthic foraminifera indicate a rapid deepening of an oxygenated marine shelf environment for the base of the section. A prominent limestone package suggests a regressive event, after which a deep, more stressed seafloor environment with less oxygen and more organic matter supply was established. Benthic assemblages suggest variable water depths between ~25 and 300 m for the studied interval (Pezelj et al., 2013). Calcareous nannoplankton data indicate an age younger than the Last Common Occurrence (LCO) of *Helicosphaera waltrans* for the transgressive base (< 14.357 Ma; Abdul Aziz et al., 2008). The LCO of *Sphenolithus heteromorphus* could not be determined precisely, but the Last Occurrence (LO) of *Sphenolithus heteromorphus* was recognized around 63 m (NN5/NN6 boundary after Martini, 1971) (Pezelj et al., 2013).

3. Material and methods

3.1. Section

The present work includes data from two partially overlapping parallel sections in the Bogutovo Selo open pit mine in Ugljevik

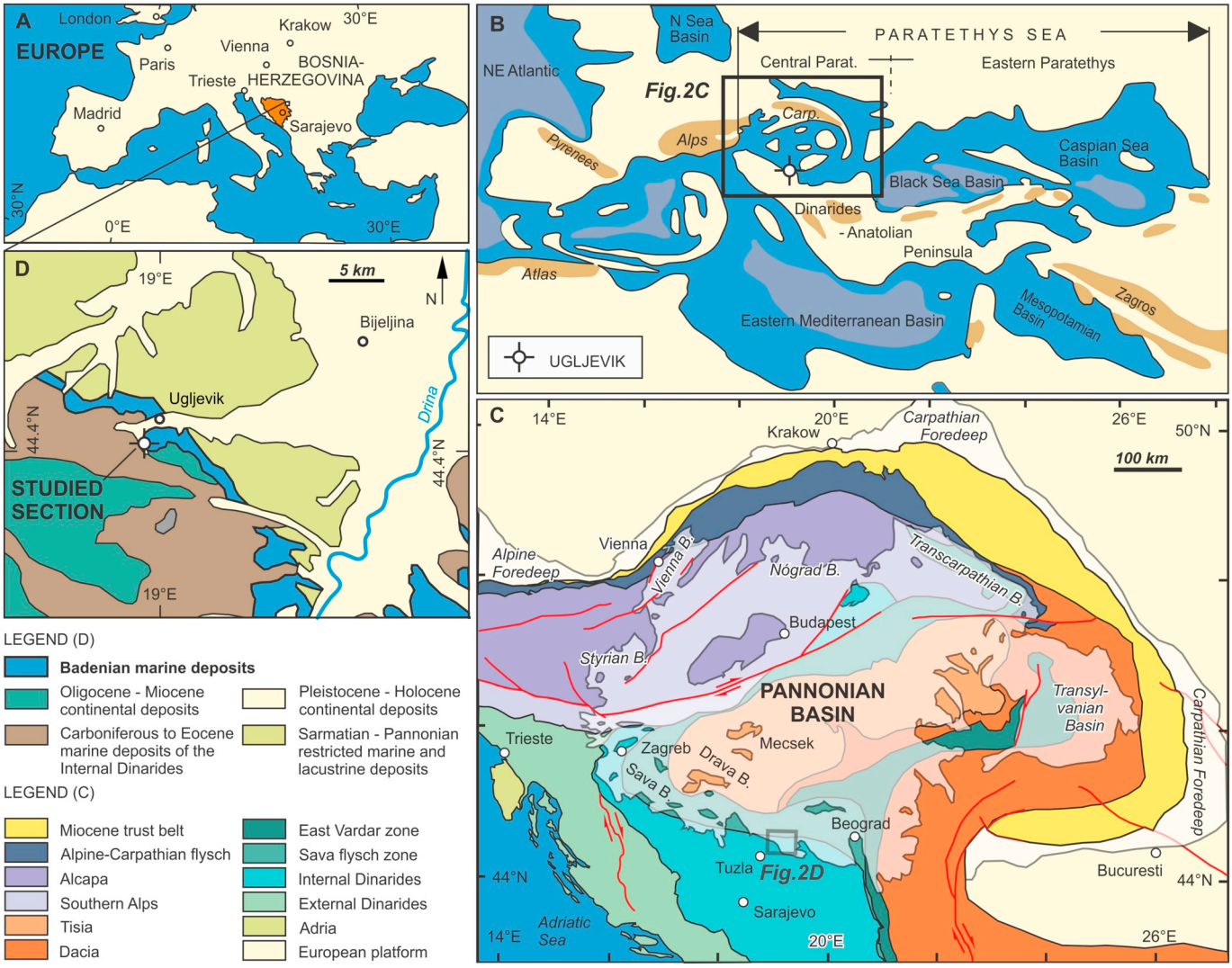

Fig. 2. Regional geological and paleogeographic setting of the study area. A. Geographic position of Bosnia and Herzegovina in Europe. B. Paleogeographic map of the Badenian (modified after Popov et al., 2004 and Palcu et al., 2017). C. Geotectonic setting of the Pannonian Basin (modified after Schmid et al., 2008). D. Geological map (modified after Geological map of former Yugoslavia, M 1: 500,000) with indicated position of study section.

(Fig. 2D), which is an active mining area (known as Prokos or Spasine) with changeable outcrop conditions due to quarrying work. Section 1 was logged in 2008 and has been presented in Pezelj et al. (2013). It collapsed in 2011 producing an escarpment located ca. 20 m to the NW of its former track and continuing to new quarry platforms. The fresh slope provided excellent outcrop conditions where a new section (Section 2; base: 44.673632°N 18.982292°E, top: 44.676939°N 18.984333°E) was logged and sampled in several field campaigns between 2011 and 2014. The section continued along the platform walls up to a Sarmatian ash layer exposed along the E-W striking road representing the fourth platform in uphill direction. Despite some small-scale WNW-ESE striking normal-faults, the fresh outcrops could be easily correlated by marker beds.

3.2. Geophysical logging

Gamma ray (GR) and magnetic susceptibility (MS) measurements were taken with a hand-held Compact Gamma Surveyor scintillation gamma radiometer (GF Instruments, Brno/Czech Republic) and an SM-30 MS meter with a sensitivity of 10^{-7} SI units (ZH Instruments, Brno/Czech Republic). Continuous measurements were taken at a mean resolution of 8 (GR) and 7 cm (MS), respectively.

3.3. Paleontology

Samples for calcareous nannofossil study were taken at a mean distance of 2 m in all lithologies except for the limestones. A detailed survey was carried out on smear slides prepared from 67 samples, of which the lowermost 28 were briefly discussed in Pezelj et al. (2013). They were examined under a light microscope, in cross and parallel light, at 1000× magnification. Sediment bulk samples (~150 g), taken every ~5 m between 80 and 135 m height, were first set in a weak hydrogen peroxide solution for several hours and then washed with tap water over 0.063—0.250 mm mesh sieves. Foraminifera were picked from the > 0.063 mm size fraction and evaluated qualitatively to close the gap with the already available record (Pezelj et al., 2013; Vrabac et al., 2015). Mollusk data were collected on site; qualitative samples for detailed taxonomic evaluation were taken where necessary. All studied material is kept in the collection of the Natural History Museum Vienna, Geological-Paleontological department, except for the calcareous nannoplankton, which is stored at the Austrian Geological Survey.

3.4. Stable isotope measurements

$\delta^{18}O$ stable isotope measurements were made on 60 bulk sediment

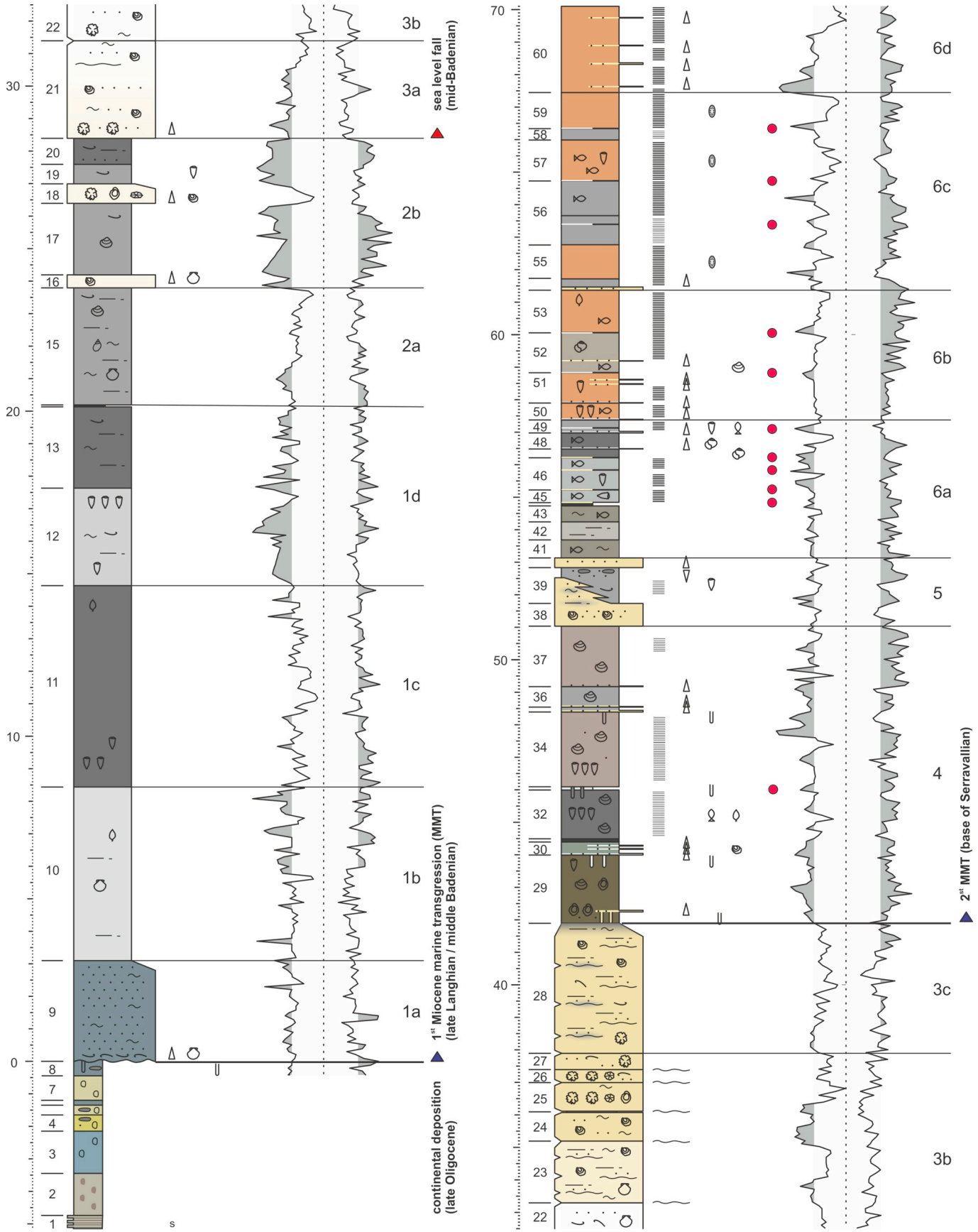

Fig. 3. Overview of the main lithostratigraphic units, lithology, fossils, MS and GR logs of the composite section in the Ugljevik mine.

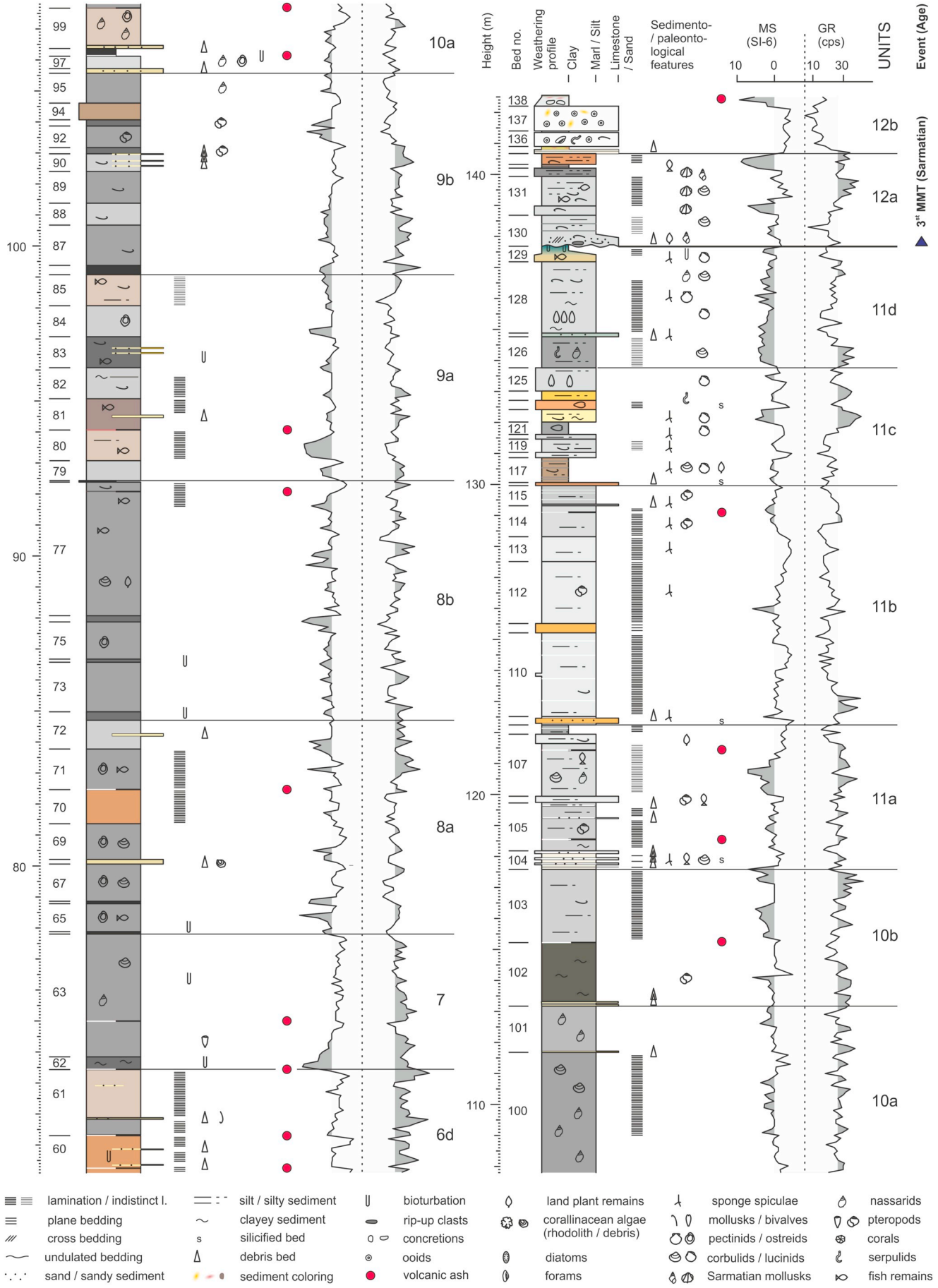

Fig. 3. (*continued*)

samples ($\delta^{18}O_{bulk}$) from two marly intervals below and above the platform carbonates (1–28 m and 42–62 m, respectively). These measurements provide additional information on the paleoclimate. Parallel isotopic analyses of $\delta^{18}O$ and $\delta^{13}C$ were performed at the Institute for Earth Sciences, University of Graz, using an automatic Kiel II preparation line and a Finnigan MAT Delta Plus mass spectrometer. Samples were dried, homogenized with a mortar, and reacted with 100% phosphoric acid at 70 °C. Analytical precision, based on replicate analysis of international standards NBS-19 and NBS-18 and the internal laboratory standard, is < 0.08‰ for $\delta^{18}O$ and < 0.04‰ for $\delta^{13}C$. Isotopic data are reported in conventional δ-notation relative to the Vienna Pee Dee Belemnite (VPDB) standard in ‰ units.

3.5. Magnetostratigraphy

A total number of 404 levels were sampled for magnetostratigraphic purposes in a composite profile (Sections 1 and 2), allowing straightforward correlation between the individual sections. Standard paleomagnetic cores were taken at 0.5–1 m resolution with a gasoline-powered electric drill using water as a coolant.

In paleomagnetic laboratory Fort Hoofddijk, rock magnetic experiments were carried out to define the magnetic carrier(s) present in the samples. Thermomagnetic measurements for 6 powdered samples were performed in air up to 700 °C on a modified horizontal translation type Curie balance (noise level 5×10^{-9} Am^2). Isothermal remanent magnetization (IRM) acquisition was performed on 24 AF-demagnetized samples using a 2G Pulser with Inline Squid magnetometer. For each specimen 60 peak fields up to 700 mT were stepwise applied, following the procedures of Kruiver et al. (2001).

Subsequently, 241 specimens were thermally demagnetized in a magnetically shielded, laboratory-built furnace with temperature steps of 20–30 °C up to a maximum temperature of 400 °C. Alternating field (AF) demagnetization was performed on 188 specimens using a laboratory-built automated measuring device applying sixteen 2–20 mT increments up to 100 mT by means of an AF-coil interfaced with the magnetometer (Mullender et al., 2016). The natural remanent magnetization (NRM) was measured after each demagnetization step on a 2G Enterprises DC Squid cryogenic magnetometer (noise level 3×10^{-12} Am^2). The paleomagnetic directions were assessed from vector end point diagrams (Zijderveld, 1967) and calculated with the least square line analysis (Kirschvink, 1980).

4. Results

4.1. Lithology and fossil content

The marine sediments in the section start with a sandy unit bearing a shell accumulation at its base (3 m; unit 1a) (Fig. 3, 4A,G,O). It grades into monotonous marl (15 m thick; units 1b-d) with alternating light and dark intervals and increased silt content in the lower and upper third. It is topped by a 6 cm-thick marker bed of dark, organic rich clay. Above, clayey, silty and sandy marls follow (8.5 m, unit 2). These are intercalated with two up to 50 cm-thick carbonate beds in their upper part (Fig. 4h). The subsequent carbonate interval (13 m, unit 3) begins with sandy corallinacean limestone with basal rhodoliths accumulations. The middle part consists of a thinning upward (2.0–0.5 m) succession of rhodolith-bearing corallinacean calcarenite (Fig. 4P). The bedding planes are undulated and marked by an increased clay content. The upper part of the carbonate interval (4 m, unit 3c) consists of silty nodular corallinacean limestone with rhodoliths and mollusk remains. It has an irregular bedding at a 1 m scale, with bedding plains marked by increased clay content. The clay component increases in the very top providing a gradual transition to the next unit (Fig. 4E).

The following unit (9 m, unit 4) is composed of green, grey and brown marls rich in mollusk accumulations, occasionally intercalated with thin biodetrital silty sand, in addition to one dark clay layer and one bentonite layer (Fig. 4E,K,M). The intercalations are intensively bioturbated. The amount of dark organic material rich sediment decreases upwards. The subsequent unit consists of two limestone beds intercalated with marl (2.2 m, unit 5; Fig. 4E,N) and has a sharp lower boundary marked by loading structures. The carbonates bear rhodoliths and mollusk fragments. The marls show indistinct lamination and bear rip-up clasts (Fig. 4N). The next unit (20 m, unit 6) starts again with greenish clayey marl and is dominated by diatomites (Fig. 4F,L). It is generally laminated and except for the very basal part intercalated at regular distance with thirteen 1 to 3 cm thick bentonite layers of volcanic origin. Two intervals in the middle and very top of the unit bear intense biodetrital sand intercalations. Fish remains are common in most parts of the unit. It is overlain by organic material rich clay and grey marl with bentonites in the base and middle part (4.5 m, unit 7). The next unit (14 m, unit 8) consists of mollusk and fish bearing grey marl. The lower part (8a) begins with two organic material rich intercalations followed by one biodetrital sandy bed. It ends with a laminated interval bearing diatomites. The overlying monotonous grey marl (8b) bears fish and plant remains, while the very top is laminated (Fig. 4C).

The following interval (7 m, unit 9a) is composed of alternating greyish and brownish marls with fish and mollusk remains and few biodetrital intercalations. The middle part bears a few biodetrital intercalations and some intervals with increased organic matter. The top consists of marls with mollusk remains (6.5 m, unit 9b; Fig. 4D) and contains a distinctive brown lithified layer. The next unit (8 m, unit 10a) starts with a bioturbated interval with 10 and 15 cm thick biodetrital fine sand beds intercalated with marl and organic rich clay. These are overlain by brownish and greyish marl, partly laminated and with common mollusks. The topmost interval in monotonous marls starts with biodetrital silt intercalations and is followed by laminated dark grey clayey silty marl (4.5 m, unit 10b).

Better lithified beds are common in unit 11. The lower interval (5 m, unit 11a; Fig. 4I) is a fining upward sequence dominated by laminated silty marl ending with a dark clay bed. It contains silicified beds and volcanic ash layers and bears mollusk and fish remains. The following interval (8 m, unit 11b) consists of laminated light grey silty marl with a dm-thick debris bed with scattered microgastropods. It is overlain by an interval with alternating grey, brown and yellowish lithified beds, silty marls and clays with frequent mollusks (debris), some serpulids and plant remains (4 m, unit 11c). The top (4.5 m, unit 11d) is dominated by laminated grey silty marl bearing mollusks and serpulids. At its very top the marl becomes lithified and brownish in colour and grades into blue-greenish clay. It bears burrows going down from the overlaying unit. Spiculae of siliceous sponges are common in the biodetrital beds and distributed in the sediment matrix throughout the topmost Badenian deposits (unit 11).

The basal Sarmatian deposits consist of cross-bedded biogenic sand rich in mollusk shell fragments (3 m, unit 12a; Fig. 4B,J), which overlies an erosive boundary forming a relief of about 10 cm height. It bears rounded mud clasts and laminae with coalified plant remains. The sand grades upwards into laminated grey silty marls bearing floating mollusks. Rare silicified and coalified wood remains up to 10 cm in diameter are present throughout the interval. The succession continues with laminated silty marl, marly siltstone with mollusk lenses, dark clay with sand intercalations and shell accumulations ending with reddish-brown laminated silt with clay interlayers. The uppermost part of the section (2 m, unit 12b) is dominated by a whitish, variegated ooid limestone containing benthic foraminifera (miliolids), serpulids and mollusks. It starts with a 23 cm interval of detrital limestone with ooids at the base, followed by brownish mudstone with reddish undulations on top. Above the ooid interval, a 30 cm-thick beige clay with carbonate concretions follows, topped by a 5 cm thick greenish to whitish bentonite with tiny mica minerals. The Sarmatian interval continues upwards with an at least 10 m thick carbonate succession (Fig. 4A).

4.2. Biostratigraphy and paleoenvironment

4.2.1. Calcareous nannoplankton

The detailed description of the trends and calcareous nannoplankton assemblages in Ugljevik based on this study and Pezelj et al. (2013) are given in Supplementary Material A. The described distribution allows the definition of four successive assemblages indicating paleoenvironmental fluctuations during marine deposition (Fig. 5):

The *Reticulofenestra minuta* assemblage marks the lower 75 m of the section. The species of which the interval bears its name dominates with a mean contribution of 74% (55–93%). The common occurrence of small reticulofenestrids such as *R. minuta* or *R. haqii* points to a nutrient-rich, eutrophic, near-shore environment (Auer et al., 2015; Haq, 1980). These opportunistic taxa have a wide ecological tolerance and are proxies of increased precipitation, freshwater influx, and terrigenous nutrient input (Aubry, 1992; Flores et al., 1995). They tolerate brackish as well as hypersaline conditions. In the Eastern Mediterranean they are associated with the Messinian evaporites (Wade and Bown, 2006), and in the Badenian stratotype section in the Vienna basin (Baden-Sooss) *R. minuta* was interpreted to reflect periods of slightly lower salinity and increased water temperatures (Ćorić and Hohenegger, 2008). The dominance of *R. minuta* in the Middle Miocene of NE Austria was related to a stratified water column (Ćorić and Rögl, 2004).

The *Umbilicosphaera jafari* assemblage marks a distinctive interval (76–94 m) of increased species richness in the section (mean 27), but with a sharp decrease in the abundance of *R. minuta*, which might indicate an intermittent period with a drier climate, temporarily increased water salinity, and shallow water depositional conditions (Ćorić and Hohenegger, 2008; Wade and Bown, 2006). The increased species richness might reflect a warmer climate, although discoasterids and sphenoliths, which prefer warm deep-sea waters and oligotrophic environments, are very rare. Their rarity might be an effect of the shallow water settings (Bartol, 2009). In the *R. pseudoumbilicus - R. haqii* assemblage, the reticulofenestrids recover their dominance, although with a changed species composition including now also larger species (Fig. 5). This assemblage marks the return to eutrophic conditions. The larger reticulofenestrids are probably the result of morphological evolution rather than of environmental conditions, because they differ morphologically from those in the basal part of the section.

The topmost 7 m of the section contains the *Coccolithus pelagicus* assemblage. The increased abundance of *C. pelagicus*, which is a cold water marker, suggests a high nutrient input and eutrophic conditions as present today in upwelling areas and/or a change of major nutrient source because of the shallowing and increasing coastal influence (Okada and McIntyre, 1979; Winter et al., 1994). Enrichment of *Helicosphaera carteri* suggests periods of turbulent water (Ćorić and Hohenegger, 2008). *Helicosphaera* spp. marks shallow water and near-shore environments (Bukry et al., 1971; Krhovský et al., 1992) and likely areas with upwelling conditions (Perch-Nielsen, 1985). Similarly to the Tisa section in the southern Carpathian Foredeep (Palcu et al., 2015), there is no major change in the nannoplankton composition across the Badenian/Sarmatian (B/S) boundary at Ugljevik (Vrabac et al., 2015).

Important stratigraphic markers in the study section are *Helicosphaera waltrans* and *Sphenolithus heteromorphus*. Only one single specimen of the first species has been detected at 1.47 m height, approving the stratigraphic position of the section above the LCO *H. waltrans* inferred by Pezelj et al. (2013). *S. heteromorphus* shows a scattered occurrence in the lower part of the section up to a height of 63 m (Fig. 5). As a result, its LCO was not easy to pinpoint, as is frequently the case in Paratethys records (e.g., Bartol, 2009; Ćorić and Hohenegger, 2008; Ćorić and Rögl, 2004; de Leeuw et al., 2018). Nevertheless, high-resolution evaluation of the critical interval enabled us to confidently fix the LO *S. heteromorphus* at 63 m height (Fig. 5).

4.2.2. Foraminifera

The foraminiferal results from Pezelj et al. (2013) (samples UG08-129 to 110), this study (samples UG14-68.3 to UG12-33) and Vrabac et al. (2015) (interval 117–141 m) and their implications for the paleoenvironment in Ugljevik are discussed below (Figs. 5, 10). See Supplementary Data A for a detailed description of foraminiferal content.

The lowermost part of the section up to 23.3 m belongs to the regional 'Upper Lagenidae Zone' (Lower Badenian sensu Papp et al., 1978) and contains abundant planktonic and benthic foraminifera typical for an oxic marine shelf environment. The following *Spirorutilus* Zone shortly predates the base of the 14 m-long carbonate platform interval (Pezelj et al., 2013). The *Spirorutilus* Zone above the latter interval is characterized by abundant benthic and planktonic foraminifera (a.o. *Orbulina suturalis*). It is dominated by benthic species such as *Bulimina subulata*, *B. elongata, Valvulineria complanata* and *Uvigerina venusta*. In contrast to the underlying ecozone it is marked by decreased species richness and increased dominance of stress markers, deep infauna and indicators of high primary production.

The transition to the *Bulimina-Bolivina* Zone in the interval 62.4–69.0 m is marked by the first occurrence of *Pappina neudorfensis*. Additional zonal marker species such as *Bolivina dilatata maxima*, *Bulimina elongata longa* and *Velapertina indigena* are recorded in the middle part of the Zone, characterized also by an interval with a maximum abundance of *O. suturalis* at 95.1–100.1 m, suggesting deep open marine conditions. The zone shows abundant and well preserved planktonic and benthic foraminifera up to 115.7 m height. Abundant uvigerinids, buliminids and bolivinids imply unstable bottom conditions and increased primary production in deeper water depositional settings. At 80.4 m height, an increased abundance of elphidiids marks a short-term installation of shallower, higher oxic depositional conditions. A similar event was found at 105–110 m by diminished plankton diversity and dominance of small globigerinids.

The top of the section (115–135 m) contains the impoverished *Bulimina-Bolivina* Zone and coincides with highly abundant sponge spiculae in the sediment continuing up to the Sarmatian boundary. The lowermost three samples bear no foraminifera, probably due to diagenetic leaching. Its upper part showed only tiny and poorly preserved benthic foraminifera. Vrabac et al. (2015) recorded foraminifera throughout the interval and interpreted it as the photic zone up to 80 m water depth. Only the very last sample, just beneath the B/S boundary, was classified to the uppermost Badenian *Ammonia viennensis* Zone by the latter authors, indicative of brackish to hypersaline lagoons (Murray, 1991). Finally, the lowermost Sarmatian part (Unit 12a) was attributed to the *Anomalinoides dividens* Zone and interpreted as low intertidal to shallow subtidal setting (Vrabac et al., 2015).

4.2.3. Mollusks

Forty different mollusk (gastropods, bivalves and nautilids) species were identified in the section. They are well preserved in marly deposits while only steinkerns and molds of the aragonite representatives are preserved in the limestones. They were assigned to eight assemblages based on their abundance distribution (Fig. 5). Except for the topmost one, all assemblages indicate a Badenian age. In particular, *Gigantopecten nodosiformis and Aequipecten elegans* are Badenian index fossils (Mandic, 2004). The presence of *Mohrensternia* sp. in the basal Sarmatian interval indicates a position within the lowermost Sarmatian mollusk biozone (Mandic et al., 2008).

The *Costellamussiopecten* assemblage is restricted to the lowermost 10 m of the section and is marked by presence of the bivalve species *C. badense* and *C. koheni*. *C. badense* is already recorded in the transgressive lag at the base of the section that also includes shallow water bivalve species such as *Aequipecten scabrella* and *Gigantopecten nodosiformis* (Mandic, 2004). Above the lag, specimens in life position are accompanied with deposit feeding bivalves such as *Nucula nucleus* and *Tellina* sp. pointing to a deepening trend and installation of calm marine settings.

(caption on next page)

Fig. 4. Photographs of the section with lithological details. A. Overview of the section of the year 2011 showing light-grey platform carbonates in the center of the picture, overlain by the grey marly succession and the light-brown Sarmatian carbonates in the top-left. B. Badenian-Sarmatian boundary. C. Left side of the photograph shows the grey marl succession of Units 7 to 10a. D. Alternation of dark clayey and light lithified marl beds. E. Interval between the platform carbonates (Unit 3) and the debris beds of Unit 5 intercalated by one ash layer (bed #33). F. Diatomites of Units 6b and 6c. G. Basal part of the section with indicated position of the Badenian lower boundary; bottom right of the picture shows a coal seam intercalated to Oligocene terrestrial-lacustrine succession. H. Interval beneath Unit 3 showing dm-thick carbonate debris layers and organic rich dark interlayer in the bottom of the illustration. I. Whitish debris bed (#104) dominated by siliceous sponge spicule intercalated to laminated marl; in the upper part a thin volcanic ash layer is intercalated. J. Sarmatian sand with mollusk debris in erosive contact with Badenian green-grey undulated clay; dark laminae within the sand are coalified plant accumulations. K. Pteropod (*Vaginella austriaca*) accumulation on the bedding plane of the bed #32. L. Diatomite laminae of bed #55. M. Dark grey volcanic ash layer (bed #33) intercalated to massive marl interval. N. detail of multiphase carbonate debris layer with central part (bed #39) showing rip-up clasts from greenish clay. O. Marine shell accumulation on top of brecciated terrestrial green marl marking the marine transgression surface of the Badenian sea. P. Detail of platform carbonate made of coralline algae fragments, with up to 5 cm large rhodoliths and a single ostreid bivalve shell. (For interpretation of the references to colour in this figure legend, the reader is referred to the web version of this article.)

The *Gigantopecten nodosiformis - Hyotissa hyotis* assemblage is bound to the carbonate intervals and represents shallow water carbonate platform conditions at depths of about 30 to 50 m (Pezelj et al., 2013). The assemblage is accompanied by the presence of colonial corals and thick-shelled bivalves pointing to increased energy conditions.

The *Neopycnodonte navicularis* assemblage has its lowermost occurrence directly above the carbonate unit at 42 m height. Between heights of 78 m and 98 m it is occasionally present as well. Rare occurrences of bivalve *Atrina pectinata*, and gastropods *Semicassis laevigata* and *Euspira helicina* were recorded as well. The name bearing species of the assemblage is closely related with the oyster *Neopycnodonte cochlear* living in the euphotic zone between 45 and 250 m in the present-day Mediterranean and NE Atlantic, where they are attached to hardgrounds at muddy gravel bottoms (Poppe and Goto, 1993; Wisshak et al., 2009).

The *Corbula gibba* assemblage has a sporadic occurrence in up to 7 m long intervals at heights of about 25 m, 50 m, 75 m, 90 m, and 120 m. It is sometimes associated with nassarid gastropods and in the interval 24 m and 48 m, the assemblage is accompanied by pteropod (planktonic gastropods) accumulations. Such a low diversity assemblage dominated by *C. gibba* species, which is capable to survive depleted oxygen conditions, indicates phases of extreme bottom conditions triggered by oxygen depletion (Mandic and Harzhauser, 2003).

The *Vaginella austriaca - Limacina valvatina* assemblage is represented in more or less continuous intervals within the lower, middle and upper part of the section, comprising all together about one third of the section's length. The planktonic gastropod *Vaginella austriaca* dominates the lower and middle intervals (8 to 75 m) and disappears before the upper one (95 to 130 m), which is exclusively represented by the gastropod *Limacina valvatina*. The latter species shows its first occurrence in the middle part of the section at level 56.3 m. Except for those planktonic gastropod species other mollusks are largely absent in the assemblage, pointing to deep water and/or hostile environmental conditions marked by bottom dysoxia. The gastropods commonly occur as pavements on bedding planes, suggesting periods of increased primary production due to a boost in nutrients. The nutrients might be of terrestrial origin and the result of humid climate intervals, or bounded to upwelling processes bringing deep water to the surface (Grunert et al., 2010).

The *Nassarius illovensis* assemblage is restricted to the upper part of the section within a single interval between 104 m and 112 m height. *N. illovensis* is usually accompanied by *C. gibba*. Gastropods *Euspira helicina*, *Aporrhais* sp., *Clavatula* sp., and lucinid bivalves *Myrtea spinifera* or *Lucinoma borealis* can be additionally present. Furthermore, *Neopycnodonte navicularis* is common at 106 m and might indicate a short-term shallowing. The assemblage represents most likely an offshore facies typical for a muddy bottom. The name-bearing species belongs to the nassarids which are scavengers living partly burrowed in bottom sediment between lower intertidal and offshore settings usually up to 300 m depth (Galindo et al., 2016; Tallmark, 1980). Morphologically similar species *Nassarius semistriatus* lived in offshore environments in Italy during the Pliocene (Dominici et al., 2018).

The uppermost 8 m-thick Badenian interval is characterized by the *Lucinoma borealis* assemblage (Fig. 5). Lucinid bivalve L. *borealis* is the most abundant species and is commonly present in life position. In addition, *Microloripes dentatus* and *C. gibba* are present, with the latter showing some extraordinarily large individuals. The assemblage is occasionally supplemented by *N. illovensis* and in the penultimate bed before the B/S boundary also by *Aequipecten elegans* and *Pecten besseri*. The majority of these species are capable to survive oxygen depleted conditions. The lucinids bear sulphur-oxidizing bacteria and are commonly present at sea grass meadows (Barnes and Hickman, 1999). Corbulids are a pioneering group able to survive short-term anoxic events at the sea bottom (Mandic and Harzhauser, 2003). Hence, the *Lucinoma borealis* assemblage suggests depleted oxygen conditions at the sea bottom and anoxic events for the topmost Badenian interval.

Finally, the *Modiolus incrassatus* assemblage is present in the Sarmatian part of the section. Except for the name bearing bivalve species, the cockle *Plicatiforma pseudoplicata* is also common. The lower part is characterized by the presence of gastropods *Mohrensternia* sp., *Turritella sarmatica* and *Gibbula* sp., and the upper part by the infaunal bivalve *Abra reflexa* and microgastropods belonging probably to *Hydrobia* sp. The lower part also comprises reworked Badenian species, such as large sized *C. gibba*. The assemblage marks shallow water (lower intertidal to shallow subtidal) conditions (Mandic et al., 2008). It is representative of the Sarmatian endemic polyhaline fauna shaped by the major extinction event known as BSEE (Harzhauser and Piller, 2007). It goes back to the installation of restricted marine conditions at the Badenian/Sarmatian transition and marks a distinct change of ecological parameters towards unstable, fluctuating environmental conditions in the Sarmatian (Piller and Harzhauser, 2005).

4.2.4. Stable isotope data

$\delta^{18}O_{bulk}$-values follow an overall trend towards heavier values upsection. The record shows a clear two-fold development above and below the carbonate deposits. In the lower part, values range from −1.48‰ to −0.12‰ (mean = −0.61‰; σ = 0.32‰). In the upper part, values increased and range from −0.45‰ and 1.07‰ (mean = 0.08‰; σ = 0.34‰) (Fig. 6).

In the lower part of the section, the $\delta^{18}O$ signal suggests relative warmer environmental conditions, while the higher values above the carbonate body hint at cooler water temperatures. The ranges of isotopic values ($\delta^{18}O_{bulk}$: −1.48‰ to 1.07‰; $\delta^{13}C_{bulk}$: −1.85‰ to 1.76‰) are similar to synchronous bulk values from the southern Vienna Basin and the Mediterranean (Kováčová et al., 2008). We thus consider diagenetic alteration to be minor or absent as it would have resulted in a significant lowering of $\delta^{18}O_{bulk}$- and $\delta^{13}C_{bulk}$-values compared to the above mentioned reference areas.

4.3. Magnetostratigraphy

4.3.1. Rock magnetic and paleomagnetic results

The thermomagnetic curves generally show a gradual, reversible decrease in intensity up to ~400 °C, when a sudden increase in intensity is followed by a decrease between 480 and 580 °C, indicating the build-up of magnetite at the expense of thermal breakdown of pyrite

Fig. 4. (*continued*)

(Fig. 7A). A small decrease around 670 °C suggests the breakdown of hematite. No indications for iron sulfides, such as greigite, were found.

The normalized IRM acquisition curves have a similar trend and a best fit was obtained using three components, fitted to the saturation isothermal remanent magnetization (SIRM), remanent coercivity force ($B_{1/2}$) and dispersion parameter (DP) (Fig. 7B). The main component is

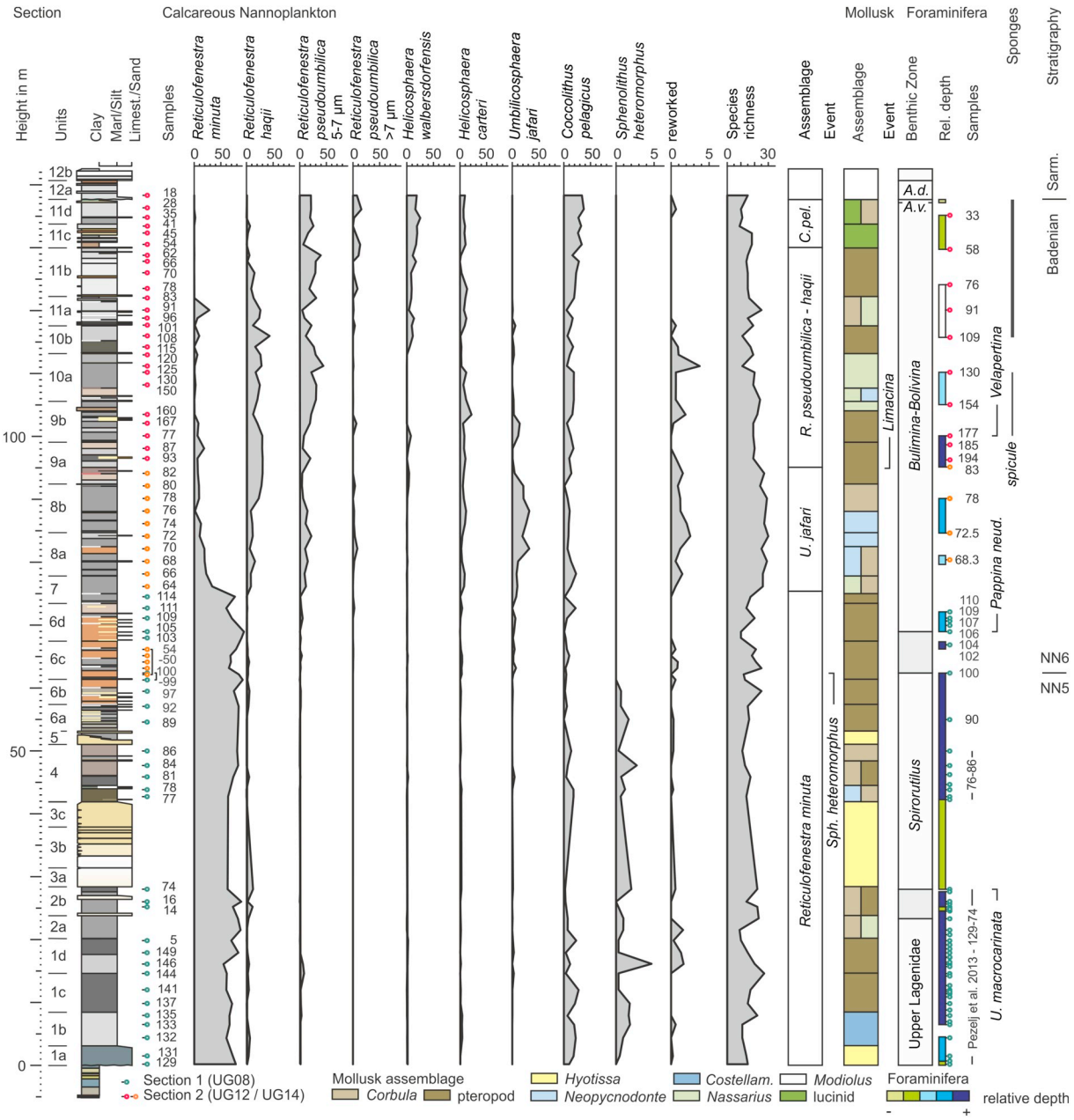

Fig. 5. Paleontological samples and results of calcareous nannofossils (includes abundance of the main species), mollusks (characteristic assemblages) and benthic foraminifera (ecozones) of the Ugljevik section.

fitted in the medium field interval, and has an average $B_{1/2}$ of 52.7 mT, DP of 0.35 and SIRM of 5.50*10–7 Am^2. This component makes up for ~93% of the total magnetization. Based on the high and variable dispersion parameter (between 0.30 and 0.43) and remanent coercivity forces (between 43.7 and 58.9 mT), we conclude that the main magnetic component of the Ugljevik section is partially oxidized magnetite of detrital origin (Hüsing et al., 2009; Kruiver et al., 2001, 2003). Note that the IRM data for the whole Ugljevik section contained a significant amount of scatter, mainly visible in the GAP plots, preventing more detailed analysis of the rock magnetic properties in the section.

As predicted by the rock magnetic analyses, the NRM intensities of the Ugljevik samples were generally low (~1000 µA/m) throughout the entire dataset. The thermal demagnetization diagrams show two or three magnetic components (Fig. 7C–I). After removal of a viscous component between 20 and 100 °C, a normal polarity component is often removed in the T-range 100–180/190 °C (e.g. Fig. 7D). Further demagnetization reveals a higher temperature component, which is stable from 180/190 °C up to a minimum of 240 and maximum of 400 °C, and can carry a reversed or normal direction. During AF-demagnetization, a low-coercivity present-day field component was removed between 5 and 20 mT. A high-coercivity component is demagnetized between 30 and 50 mT (Fig. 7F). The paleomagnetic data files are found in Sant et al. (2018b).

In general, thermal demagnetization (TH) provided higher quality results than alternating field demagnetization (AF). AF demagnetization especially proved to be less suitable to completely remove the present-day field overprint, as earlier also shown for Sarmatian samples of the Pannonian Basin (ter Borgh et al., 2013). A Characteristic Remanent Magnetization (ChRM) direction is considered reliable if it includes at least 4 consecutive data points, linearly decays towards the origin, and lies in the temperature range 180–390 °C or in the coercivity range 25–80 mT. In total, 65% of the thermally demagnetized samples and 50% of the AF-demagnetized samples qualify as reliable. Another 30 samples show a trend towards reversed polarity, but have a lack of

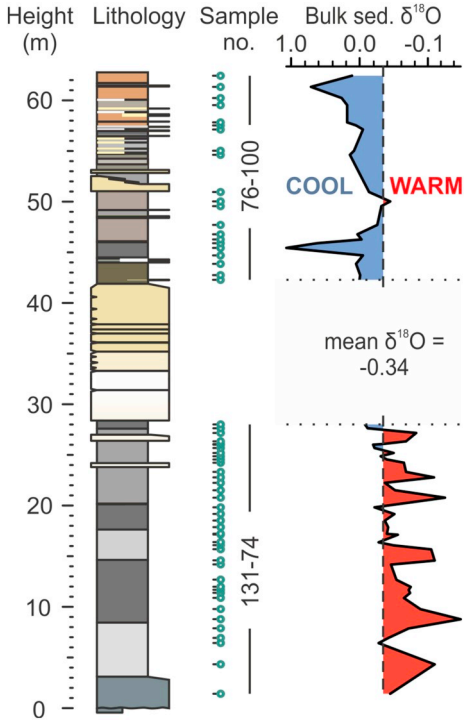

Fig. 6. $\delta^{18}O$ isotope data from bulk sediment samples at the base of the Ugljevik section.

linear decay towards the origin. In these cases, the ChRM was extracted using great circle analysis (McFadden and McElhinny, 1988), but only if the sample was located in a zone with reliable reversed polarity samples (Fig. 7I,J).

The mean inclination of the high temperature/coercivity directions in tectonic coordinates ($I = 44.2$) is significantly shallower than the expected inclination for Ugljevik in the middle Miocene (Torsvik et al., 2012) (Table 1, Fig. 7K,L). This suggests that the inclination of the samples was flattened by compaction and dewatering of the sediment. Application of the Elongation/Inclination method (Krijgsman and Tauxe, 2004; Tauxe and Kent, 2004) on our dataset gives an E/I corrected inclination of 61.6 [54.9, 70.7], which is in excellent agreement with the expected inclination of 60.2° (Fig. 7M,N). This shows that the high temperature/coercivity magnetic directions were acquired before dewatering and compaction of the sediments and represent the ChRM.

4.3.2. Polarity pattern

The quality of the demagnetization results varies significantly throughout the Ugljevik section. Weaker samples occur in the whole section, but are increasingly more abundant above 85 m (Fig. 8). Besides a slightly lower magnetic intensity in the upper part, the difference might be caused by a different preservation of the magnetic minerals (e.g., further oxidized magnetite) or a mix of magnetic minerals (e.g., an iron sulphide with magnetite). However, the general low intensity of the samples did not allow for a more detailed rock magnetic investigation to unravel the cause for the different behavior. The polarity pattern in the upper part could still be determined by high resolution magnetostratigraphy.

Plotting the ChRM directions in stratigraphic order reveals the presence of 12 polarity zones (R1 – R6) and 11 reversals (Fig. 8). The locations of the reversals are based on reliable samples only. In case of conflicting TH and AF directions, the TH directions were given priority.

Two reliable normal polarity samples are present immediately above the basal unconformity, followed by a reversed zone (R1; 4–13 m) (Fig. 8). The reversal coincides with a facies change from fine-sandstone to marl. As coarse-grained facies commonly yield lower quality ChRMs than fine-grained facies, the polarity in the lowermost 3 m should be treated with caution, and is marked grey in the polarity column. The interval 3–104 m contains well-defined polarity zones with clear reversal boundaries (N1, R2, N2). From 104 m upwards, the intensities are lower and the directions less consistent, especially for the reversed polarities (Fig. M3). Still, two reversed intervals (R3 and R4) and one normal polarity zone (N3) could be interpreted between 104 and 112 m, whereas the interval 112 to 128 m is unclear. This part contains two normal (N4 and N5) and one small reversed zone (R5), or only one normal zone (N4). The uppermost part, including the B/S boundary, contains a clear reversed zone (R6), and is finalized by a normal one (N6).

5. Discussion

5.1. Bio-magnetostratigraphy, correlation to the GPTS and sedimentation rates

The magnetostratigraphy of the Ugljevik section is correlated to the astronomically dated Geomagnetic Polarity Time Scale (GPTS) of Hilgen et al. (2012) (Fig. 8). The bio- and event stratigraphy of the section provides important tie points for correlation. First of all, the base of the Badenian succession should be younger than 14.357 Ma, according to the astronomically dated LCO of *H. waltrans* in the Mediterranean (Abdul Aziz et al., 2008). In the Paratethys, its common occurrence is restricted to the Lower Lagenidae Zone (Ćorić et al., 2007). Second, the LO of *S. heteromorphus* (NN5/NN6 boundary) at 63 m should approximate the ages for the LO in the open ocean (13.53 Ma; Backman and Raffi, 1997) and the LCO in the Mediterranean (13.65 Ma; Mourik et al., 2011). Third, the B/S boundary was recently bio-magnetostratigraphically dated at 12.65 ± 0.01 Ma (Palcu et al., 2015). In Ugljevik, the boundary is expressed by an omission surface. A long-term hiatus is unlikely because the topmost Badenian and lowermost Sarmatian biozones are detected below and above the gentle erosional surface. This suggests that the reversed polarity in the lower part of the Sarmatian strata belongs to the same Chron as the one in the uppermost Badenian.

Accordingly, R1 at the base of the marine section is correlated to Chron C5ACr, followed by the correlation of N1 to Chron C5ACn (Fig. 8). The LO of *S. heteromorphus* is present at 63 m in the subsequent reversed polarity interval R2, which we accordingly correlate to Chron C5ABr (13.75–13.60 Ma). Subsequent normal polarity interval N2 logically correlates to C5ABn. Despite the overall weaker results above 85 m R3 can be convincingly correlated to C5AAr, N3 to C5AAn and R4 to C5Ar.3r. Since the reversed polarity of R5 is uncertain, two different correlations were made for the interval between 111 and 128.5 m (Fig. 8). In the first one, N4, R5, and N5 are tied to the C5Ar.2n, C5Ar.2r, C5Ar.1n interval of the geomagnetic polarity timescale. In this case, the B/S boundary falls within Chron C5Ar.1r. However, reversed interval R5 is only indicated by a single reversed sample and hence relatively poorly established. It would, therefore, alternatively be possible to tie the complete N4, R5 and N5 interval to the short normal Chron C5Ar.2n. This alternative correlation would place the reversed polarity interval of the B/S boundary in Chron C5Ar.2r.

With the proposed magnetostratigraphic correlation the mean sedimentation rates per interval can be calculated (Fig. 9). Sedimentation rates in the 0–50 m interval are slightly higher than 11 cm/kyr, while in the middle part of the section (50–92 m) sedimentation rates range between 4.7 and 7.6 cm/kyr. The mean sedimentation rate for the upper part of the section (92–143.5 m) was not calculated because of the weaker polarity zonation in this part. The elevated sedimentation rates in the lower part of the section could indicate a higher supply of material in general, possibly because of a slightly higher subsidence rate or a higher input from the mainland.

Sedimentation rate calculations help to decide between the two correlation options. Correlation option 2 leads to a sedimentation rate

of approximately 27.5 cm/kyr for the N4, R5 and N5 interval. This rate is about three times higher than the average depositional rate in the rest of the section. Correlation option 2 is, therefore, unlikely. We adopt correlation option 1, which results in a much more reasonable sedimentation rate of 11 cm/kyr. Along these lines, the B/S boundary falls within C5Ar.1r and has an age between 12.735 and 12.474 Ma (Hilgen et al., 2012).

5.2. Sea-level change and environmental history in Ugljevik

A sequence stratigraphic interpretation for the lower part of the section was introduced by Pezelj et al. (2013). The present study confirms and supplements their interpretation. The new paleontological, isotopic and geophysical (MS, GR) data furthermore allow to extend the interpretation to the whole Badenian succession, which can be

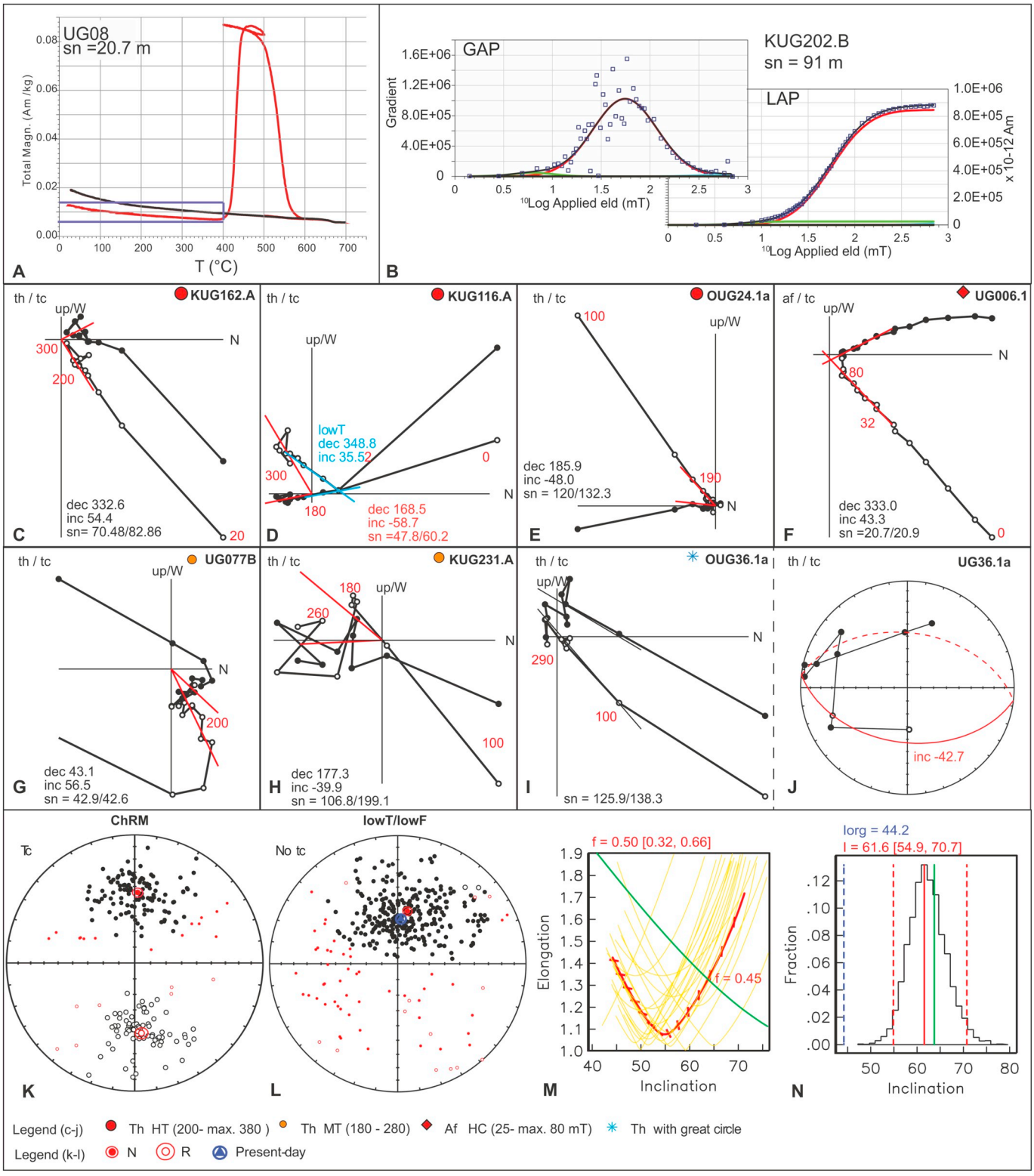

(caption on next page)

Fig. 7. A. Thermomagnetic curve displaying an increase between 400 and 580 °C indicating the growth of magnetite at the expense of thermal breakdown of pyrite. Red (black) intervals show heating (cooling). B. An isothermal remanence magnetization (IRM) acquisition curve fitted to a linear acquisition plot (LAP) and gradient acquisition plot (GAP) (Kruiver et al., 2001). Squares represent data points plotted logarithmically, the red line is the best fit for component 1, the green line for component 2, the blue line for component 3 and the black line represents the sum of three components. See text for further explanation. C–J. Representative Zijderveld diagrams (C–I) and equal area projection (J) of thermally (th) and alternating field (af) demagnetized samples throughout the Ugljevik section. Closed (open) circles represent declination (inclination) data points. Red values denote th (af) steps. Red (blue) lines are primary (lowT) directions. HT (MT) = high (medium) temperature range. HC = high coercivity range. tc = tectonic correction. no tc = no tectonic correction. sn = stratigraphic level in sub-section/composite section. Sample codes and quality are noted in upper left corners. (J) Shows the plotted great circle for sample OUG36.1a. K–L. Equal area projections including all reliable directions (ChRM) and low temperature/low field directions for the composite section. Closed (open) circles denote normal (reversed) inclination. Red circles are outliers determined with the Vandamme cut-off (Vandamme, 1994) and are not taken into account when calculating the mean directions. (No) tc = (no) tectonic correction applied. M–N. Result of the Elongation/Inclination method (Tauxe and Kent, 2004) produced by the program TK03_GAD.exe. (M) displays one example of the > 1000 model fits, which are all taken into account to estimate the flattening factor ('f') and new inclination ('I') after decompaction. In (N) the 95% error bar is marked with vertical, dashed red lines. The blue dotted line shows the original inclination (Iorg). This line plots well outside the 95% range, so the new inclination is statistically significant. (For interpretation of the references to colour in this figure legend, the reader is referred to the web version of this article.)

confidently divided into four Transgressive-Regressive (T-R) cycles (Fig. 10). The upper and lower boundary of the Badenian mega-cycle are marked by erosive omission surfaces and hiatuses. The rest of the marine succession shows continuous subaquatic deposition. Cycle boundaries are not expressed as sharp erosional surfaces. We, therefore, integrated lithofacies and biofacies indicators to define the most probable positions of corresponding sea-level minima. According the our age model, the cycle boundaries roughly coincide with 400 kyr eccentricity cycles, whereas the Serravallian part of the Badenian mega-cycle corresponds to a single 1.2-Myr obliquity cycle (Figs. 1, 10).

5.2.1. T-R 1

The first T-R cycle is marked by a transgressive lag followed by rapid deepening represented by the foraminiferal assemblages of the Upper Lagenidae Zone and *Costellamussiopecten* mollusk assemblage. The start of the highstand systems tract (HST) is correlated with the first terrestrial input in the section at a height of 8 m.

5.2.2. T-R 2a

The prominent coralline limestone interval, including colonial coral remains, marks the installation of a carbonate platform and the lowstand systems tract (LST). The magnetostratigraphic age between 14.05 and 13.75 Ma and the main shift of the $\delta^{18}O$ signal towards cooler temperatures for the interval of carbonate deposition indicates that the inception of the carbonate platform correlates with the global cooling event at the Langhian/Serravallian boundary and the associated glacio-eustatic sea level drop (Mi-3b). The upwards increasing debris inflow from the carbonate platform, *Hyotissa* mollusk facies and shift in benthic foraminiferal assemblages all indicate a shallowing of the sea before and during carbonate deposition. Low MS and GR values imply decreased terrestrial input and/or increased sediment accumulation rates typical for carbonate platforms in transgressive systems (Handford and Loucks, 1993; Schlager, 2005). We suspect therefore that this interval might have a much higher sedimentation rate than the deep water marls below and above. Such a short duration of carbonate deposition would allow for the correlation of T-R 1 cycle with a single 400-kyr-eccentricity cycle (Fig. 10). Despite the ~200 m sea level drop based on benthic foraminifera, the environment remained fully marine and relatively deep (~30–50 m; Pezelj et al., 2013). The deepening on top of the platform occurred very fast and amounts to > 100 m (Pezelj et al., 2013). This sea-level rise might coincide with the Serravallian transgression astronomically dated on Malta at 13.76 Ma (Mourik et al., 2011). The HST is marked by massive diatomite deposition, a generally increased GR signal and omnipresent planktonic gastropods. The diatom blooms might have been enhanced by an increased availability of silica in the sea water brought in by ash fall (Fig. 3). The raised GR might reflect high primary productivity, because organic matter captures uranium.

5.2.3. T-R 2b

T-R cycle 2b is defined between two shallower water intervals indicated in unit 8a and in unit 9b-c transition by thickest debris layers pointing to the closest position to coastal settings in that part of the succession. Moreover, the base coincides with the occurrence of the *Neopycnodonta* assemblage pointing to re-occurrence of relatively shallower settings. Shallow water in the lower boundary interval is indicated by a benthic foraminifera fauna bearing common *Amphistegina* and *Elphidium*, as well as by the *U. jafari* calcareous nannoplankton assemblage and a peak in reworked nannoplankton (Fig. 5). The maximum flooding surface (mfs) is set at the restart of debris input that coincides with the re-occurrence of abundant planktonic foraminifera with large *O. suturalis* pointing to deepest depositional setting within the cycle. The top is marked by a bioturbated interval with debrites and accumulations of sponge spiculae that were likely washed in from the shallow shelf. The GR trend slightly follows the precession trend, especially notable in Units 9a and 9b (Fig. 10). Diversified

Table 1
Mean declination and inclination values, and α95 in degrees (°) determined with the Vandamme cut-off (Vandamme, 1994) for all reliable directions and (expected) present-day and Miocene magnetic parameters for the study locality. N = number of data points used in analysis. (No) tc = (no) tectonic correction applied, lowT = low temperature zone. The mean normal value in no tc for the studied section is different from the present-day field on the Ugljevik locality. The inclination produced after applying the Elongation/Inclination method (Tauxe and Kent, 2004) is similar to the expected field ~ 15.0 Ma. See Fig. 7k for an illustration of the method.

Group	Normal				Reversed			
	Dec	Inc	N	a95	Dec	Inc	N	a95
Partial section 1, tc	12.1	46.0	32	6.2	179.1	−50.2	19	8.6
Partial section 2, tc	359.4	43.5	88	3.5	172.7	−42.5	57	4.3
Composite section, tc	2.2	44.2	119	3.1	174.2	−44.0	73	3.7
Composite section, no tc	9.8	60.7	117	3.0	172.0	−58.7	73	4.2
LowT/low field, no tc	10.5	55.7	273	3.3				
Present-day Ugljevik	3.0	62.3 [60.7, 63.9]						
Expected Ugljevik (15 Ma)	4.8	61.8 [60.0, 63.6]						
Unflattened (Tc, N + R)	358.2	61.6 [54.9, 70.7]	189	1.8				

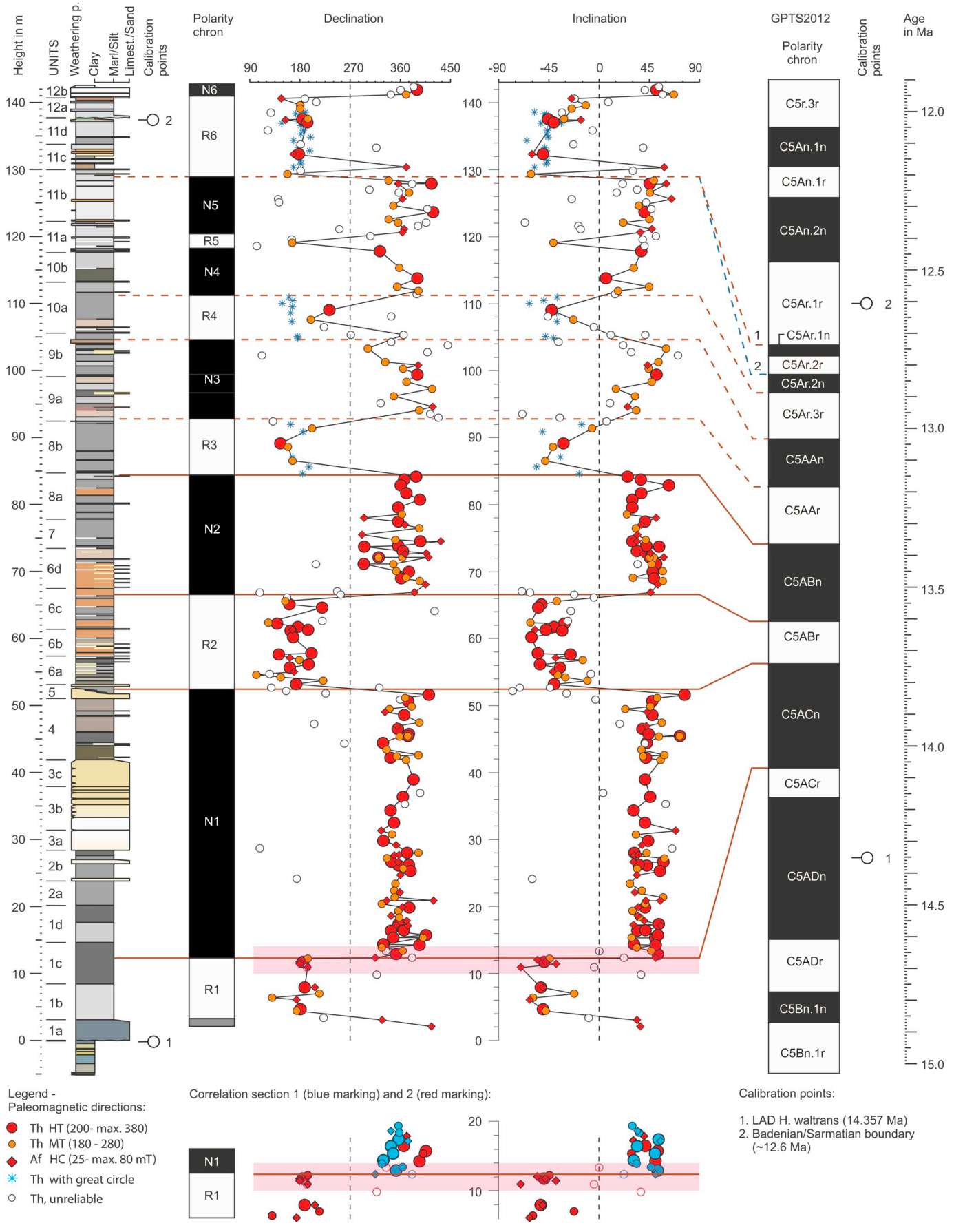

(caption on next page)

Fig. 8. Magnetostratigraphic correlation of the Ugljevik section to the GPTS (Hilgen et al., 2012). Bio-events for calibration are listed next to the section and GPTS. Black (white) zones in the polarity column indicate normal (reversed) polarity. R1 – N6 are given names for the interpreted polarity zones. N5 and R5 represent alternative interpretations of the zones. See figure legend for the symbol explanation. Two correlation options are shown for the uppermost part.

calcareous nannoplankton and the peak abundance of *O. suturalis* indicate persistence of warm water conditions within the T-R cycle (Fig. 5; Bicchi et al., 2003; Rupp and Hohenegger, 2008).

5.2.4. T-R 2c

The final T-R cycle shows a short deepening pulse. Within the transgressive systems tract (TST), both MS and GR show an increasing trend ending at the maximum flooding surface. The start of the HST is indicated by debrites in the upper part of Unit 10a and coincides with a blooming event of the planktonic gastropod *Limacina valvatoides* pointing to increased primary production. The subsequent shallower inner shelf setting is reflected by marls with masses of sponge spiculae, fish remains, and the *Ammonia viennensis* assemblage found by Vrabac et al. (2015) in the topmost Badenian bed. The latter marks the installation of brackish to hypersaline lagoonal settings and the shallowest depositional environment preserved within the Badenian succession. T-R cycle 2c ends with the B/S boundary and is characterized by a 10 cm-thick, irregular erosion horizon (Fig. 4B,J) associated with frequent coalified and silicified tree trunks and lithified Badenian mudclasts, which probably points to emersion of the area. Reworked Badenian macro and microfauna are associated with the boundary. The outcrop shares characteristics with the B/S boundary at the locality Gornje Vrapče (Zagreb) in the SW Pannonian Basin, where a marly interval with highly abundant sponge spiculae is followed by 1 m-thick limestones with an erosive surface on top (Pezelj et al., 2016).

The Mi-3b lowstand, which is very prominently expressed in our section, coincided with a period of minimum amplitudes in obliquity related to the 1.2-Myr cycle and minimum values of eccentricity as part of both the 400- and 100-kyr cycle (Abels et al., 2005). When we use the magnetostratigraphy of our section as a guideline for correlation to the polarity timescale (Fig. 10), it is evident that the other transgressive-regressive cycles at Ugljevik have exactly the same phase relation with the precession and eccentricity curves.

5.3. Badenian events: from Ugljevik to the whole Central Paratethys

5.3.1. The mid-Langhian marine transgression

The Langhian transgression at the Ugljevik locality (~14.2 Ma) has a similar age range as it has in many sections in present-day Hungary (Mecsek area, Soltvadkert Trough, Borsod Basin), where the flooding is also associated with *S. heteromorphus* and *O. suturalis*, and *H. waltrans* is absent (i.e. regional Upper Lagenidae Zone, < 14.36 Ma) (Báldi, 2006; Báldi et al., 2017; Selmeczi et al., 2012) (Fig. 2C). Beyond that, this transgression is coeval with the second T-R sequence of the Vienna Basin (Ba2 of Strauss et al., 2006), based on biostratigraphy and astronomical tuning of the Badenian holostratotype Baden-Sooss (Hohenegger and Wagreich, 2012; Hohenegger et al., 2009; Papp et al., 1978). In most basins in the rest of the Central Paratethys, including the Transylvanian Basin, Carpathian Foredeep, Vienna, Danube and Styrian basins, the widespread marine flooding is associated with *Praeorbulina glomerosa circularis* and/or *H. waltrans*, indicating a slightly older age for the onset of the Badenian flooding (~14.9–14.36 Ma) (Beldean et al., 2013; Ćorić and Rögl, 2004; Rybár et al., 2016; Spezzaferri et al., 2009). In some of these basins, terrestrial or lacustrine deposition occurred before the onset of the Badenian flooding. In others, uppermost lower Miocene (Karpatian) marine deposits are present (Sant et al., 2017).

At the southern margin of the Pannonian Basin, the progradation of the Badenian transgression shows south-eastwards rejuvenation that might be linked to the late post-orogenic history of the Dinarides (Ilić and Neubauer, 2005). In the Sava and Drava depressions (Fig. 2c), *H. waltrans* and *Orbulina suturalis* were encountered at the base of the marine deposits (~14.6–14.36 Ma) (Ćorić et al., 2009; Pavelić and Kovačić, 2018), indicating an earlier flooding, than in the eastward neighboring Ugljevik area. Furthermore, to the southeast still younger marine flooding dated to the late Badenian is present in the Morava Basin of Central Serbia (Sant et al., 2018a). These variations in the age of the flooding show that, despite the flooding of many Central Paratethys basins during the Mi-3a high stand (~14.9–14.6 Ma) (John et al., 2011; Kominz et al., 2008), the local tectonic and sedimentary basin settings provided an important control on the marine transgression.

The delayed flooding in Ugljevik suggests that tectonic subsidence was the major factor controlling the marine transgression in this region. Synchronicity with the second T-R sequence of the Vienna Basin suggests that still a sea level change might play a role as well (Strauss et al., 2006). Active rifting in the North Croatian Basins most likely continued until the mid-Badenian (~14–13 Ma), so subsidence in Ugljevik might have as well (Pavelić and Kovačić, 2018). Moreover, tectonic and sedimentary data implying a peak rifting period in the SE Pannonian basin roughly between 15 and 14 Ma (Balázs et al., 2016; Matenco and Radivojević, 2012; Stojadinović et al., 2013).

5.3.2. The lower Serravallian: stress in the Central Paratethys

In Ugljevik, the end of the MMCT and of the Mi-3b sea level drop (= base Serravallian stage) is expressed by an abrupt shift from carbonate platform conditions to deeper marine deposition (Fig. 10). The cooling is well expressed by increased $\delta^{18}O$ values above the carbonates. The drop in temperature is recognized all over the Central Paratethys by changes to temperate-cold foraminiferal assemblages and a decline in gastropod diversity (Gonera et al., 2000; Harzhauser and Piller, 2007; Peryt, 2013a). The water temperature decrease is estimated between ~2 and 6 °C (Gonera et al., 2000; Peryt, 2013a).

Almost immediately after the onset of the cooling event, thick (~10–200 m) packages dominated by salt, gypsum and anhydrite were deposited in the eastern Central Paratethys including the Carpathian Foredeep, Transylvanian and Transcarpathian/East Slovak basins (Báldi et al., 2017; Bojar et al., 2018; Bukowski et al., 2007; de Leeuw et al., 2010; Krézsek and Bally, 2006; Peryt and Peryt, 2009; Túnyi et al., 2005). The base-level drop that accompanied the global cooling event is, therefore, thought to have restricted outflow of deep saline bottom waters from large parts of the semi-isolated Central Paratethys, hence triggering the concentration of salt (de Leeuw et al., 2010). In the Carpathian Foredeep, halite precipitated from density stratified brines in the deeper parts of the basins, while gypsum precipitated at the basin margins (Babel, 2004; Peryt, 2013b). In between, an anhydrite zone developed by *syn*- and post-sedimentary alternation of the gypsum (Peryt, 2013b).

Evaporitic deposition began ~13.8 Ma and ceased between 13.6 and 13.32 Ma (de Leeuw et al., 2018, De Boer et al., 2010; including a recalibrated $^{40}Ar/^{39}Ar$ age from Śliwiński et al., 2012). In the Pannonian Basin, several up to 35 m-thick halite intervals were recognized in drill cores in Central Hungary, overlain by up to 15 m-thick anhydrite packages (Báldi et al., 2017). Such a middle Badenian succession is present also in the Tuzla Basin, SE of Ugljevik, composed of up to 180 m-thick halite interval overlain by up to 20 m-thick anhydrite package (Čičić and Jovanović, 1987; Ćorić et al., 2007). Finally, in the Vienna Basin, a > 100 m-thick unit of anhydrite-bearing clay is present overlain by the late Badenian open marine deposits (Harzhauser et al., 2018). Consequently, Báldi et al. (2017) proposed that the BSC evaporites were once very widespread in the Pannonian Basin and were only preserved in the deepest basins, overlain by younger sediments that protected them from reworking, but more observational and

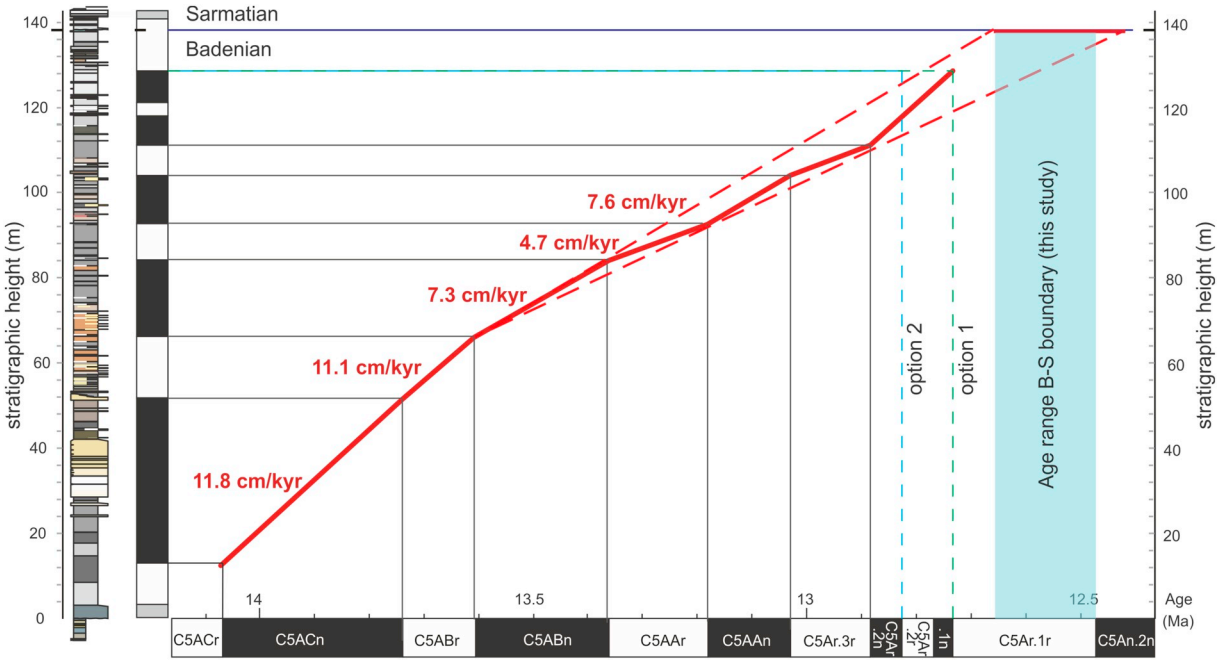

Fig. 9. Sedimentation rates (red values) along the Ugljevik section as derived from the correlated magnetostratigraphy. The red dashed lines mark the minimum and maximum estimated sedimentation rate in the upper part of the section, extrapolated from the mean sedimentation rates in the middle part of the section. The horizontal red band marks the age range of the B/S boundary deduced from this extrapolation. (For interpretation of the references to colour in this figure legend, the reader is referred to the web version of this article.)

modelling data are needed to test this hypothesis.

Benthic foraminiferal data from evaporite sections right below, within and above the salt bodies suggest enhanced vertical stratification coupled with a high-productivity surface water and increased organic flux to the bottom (e.g., *Bulimina elongata*) (Báldi, 2006; Peryt, 2013a; Peryt et al., 2014). This points to increased nutrient fluxes from the land, or by coastal upwelling of deeper water. Similar benthic foraminiferal markers (Pezelj et al., 2013) and blooms of diatoms (unit 6c) were recorded in the 20 m interval above the main carbonate body in Ugljevik (units 4–6), indicating enhanced vertical stratification. Moreover, the low diversity *C. gibba* mollusk assemblage appears for the first time just below the carbonate platform (*Corbula* in Fig. 10) and planktonic gastropods and lamination are omnipresent. This suggests phases of dysoxic bottom conditions and increased primary production between ~13.9 and 12.7 Ma. The diatom blooms occur up to max. 13.4 Ma and demonstrate that the vertical stratification in Ugljevik was most severe during evaporite deposition in the Carpathian Foredeep (Fig. 10).

The transition between the *Spirorutilus* and *Bulimina-Bolivina* Zones coincides with diatomite deposition (61–68 m) and correlates roughly with the LO of *S. heteromorphus* (=NN5/6 boundary; Fig. 10). Note that the *Spirorutilus - Bulimina-Bolivina* Zone boundary by definition marks the boundary between the middle (Wielician) and late (Kosovian) Badenian sub-stages in the Central Paratethys (Papp et al., 1978; Fig. 10). According to our age model, it correlates with the boundary between Chrons C5ABr and C5ABr and has an age of 13.61 Ma. Interestingly, planktonic foraminifera and ostracod marker species for the Wielician stage are still present in the marls that overlie the BSC gypsums in the Carpathian Foredeep, which were radioisotopically dated at 13.32 ± 0.07 Ma (de Leeuw et al., 2018).

The subsequent distinctive change to less stratified marine water is clearly noted in Units 6d-7 in Ugljevik (~13.6–13.5 Ma), containing an abrupt decrease in the stress marker *R. minuta* (start *U. jafari* assemblage) at 75 m, the end of the diatom blooms, and the beginning of an short-term phase with shallower depositional conditions.

Thus, the global cooling and Mi-3b isotope event in the Central Paratethys was associated with widespread evaporite deposition in the east (Carpathian Foredeep, Transcarpathian/East Slovak and Transylvanian basins), halite deposition in some deep depocentres of the central Pannonian Basin, and basin shallowing and erosion of marginal facies in all areas. At Ugljevik, that shallowing is reflected by the installation of platform carbonates in open marine settings, whereas the neighboring Tuzla Basin turned to a hypersaline lagoon triggering deposition of a 550 m thick evaporite succession with thick halite and anhydrite intervals (Čičić and Jovanović, 1987).

The different expressions of the cooling-induced sea level drop and subsequent period of restriction (~13.8–13.3 Ma) in the sub-basins was most probably caused by the variable tectonic and sedimentary basin settings, in combination with several sills in the Pannonian Basin. Palcu et al. (2017) argued that some brackish water from the Eastern Paratethys already spilled over into the Carpathian Foredeep during the salinity crisis, since the Black Sea Basin had a positive hydrological budget since 13.8 Ma. The unidirectional brackish water flow enhanced stratification in the eastern part of the Paratethys and contributed to the severe salinity crisis. However, the present section demonstrates that during the BSC event in the Carpathian Foredeep, the Pannonian Basin retained a fully marine ecosystem, with platform carbonates at Ugljevik, followed by deep water marls rich in planktonic foraminifera of Mediterranean affinity after the Serravallian transgression.

The ending of the BSC in the eastern part of the Central Paratethys was likely the result of progressive tectonic subsidence in the Carpathian Foredeep area and the Pannonian Basin, while the exact moment of termination was determined by a short-term sea level rise around 13.3 Ma (de Leeuw et al., 2018). As a result, shallow two-directional water exchange initiated between the Central and Eastern Paratethys and increased exchange between the Central Paratethys and the Mediterranean (Bartol et al., 2014; Palcu et al., 2017; de Leeuw et al., 2018). According to our age model, this transgression coincided with the second Serravallian sea-level rise (T-R 2b) at Ugljevik.

5.3.3. *The BSEE extinction event*

The interval below the BSEE in Ugljevik is characterized by

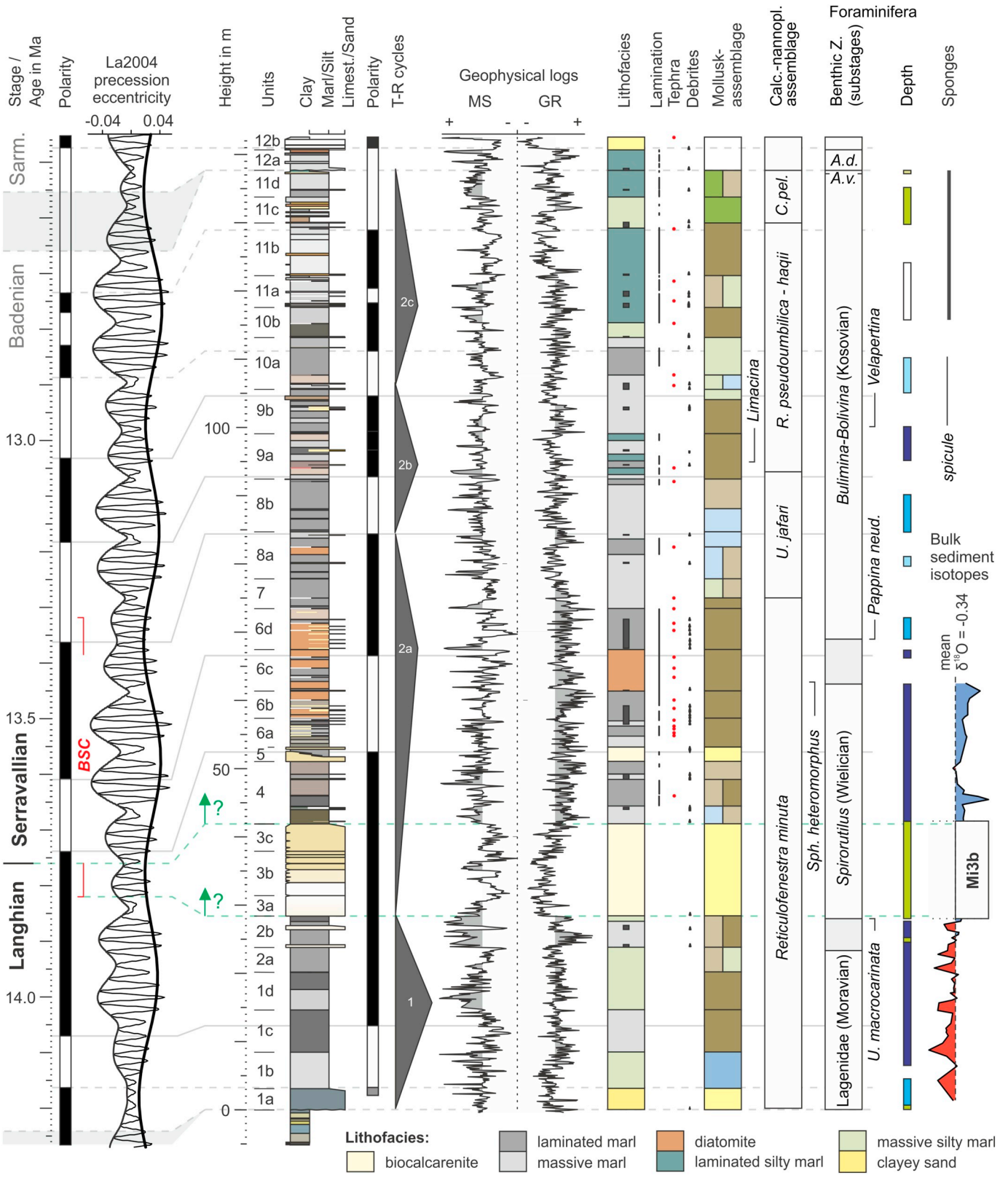

Fig. 10. Integrated stratigraphy and paleoenvironment of the Ugljevik section: magnetostratigraphic correlation, lithology, Transgressive-Regressive (T-R) cycles, magnetic susceptibility and gamma ray curves, lithofacies, mollusk facies, calcareous nannofossil assemblages, ecozones based on benthic foraminiferal assemblages and $\delta^{18}O$ isotope data.

intensively laminated silty marls with the opportunistic calcareous nannoplankton assemblage of *C. pelagicus,* and *Corbula* mollusk assemblages pointing to hostile conditions with re-occurring depleted oxygen at the sea floor. Finally, the benthic foraminifera show a shallowing upwards trend with the establishment of a brackish to hypersaline lagoon just before the Sarmatian boundary. At the base of the

Sarmatian, a rich but completely different mollusk assemblage is present. The faunal character with abundant cardiid mollusks correlates with the same interval of the Eastern Paratethys pointing to their faunal exchange. A restricted connection to the Mediterranean was possibly still present based on the establishment of polyhaline to hyperhaline environmental conditions in the Central Paratethys (Harzhauser and Piller, 2007). Although still different in species composition, the Central Paratethys Sea largely merged with the Eastern Paratethys to form one uniform Sarmatian bioprovince, completely dissimilar to Mediterranean-Lusitanian (Harzhauser and Piller, 2007; Popov et al., 2004).

The presented magnetostratigraphic age model (option 1) dates the BSEE at ~12.6 Ma (full range: 12.72–12.48 Ma). This is in agreement with the bio-magnetostratigraphic studies of Palcu et al. (2015) in the South Carpathian Foredeep, and of Paulissen et al. (2011) in the central Vienna Basin. See Palcu et al. (2015) for an extended review of dating studies on the Badenian/Sarmatian boundary.

Many B/S boundaries in marginal settings of the Pannonian Basin System are erosive (Harzhauser and Piller, 2007; 2004; Pezelj et al., 2016; Vrabac et al., 2015). That major regressive phase is noted in numerous seismic sections, interpreted as a sea level drop of ~50 to 80 m (Kováč et al., 2004; Schreilechner and Sachsenhofer, 2007; Krézsek and Bally, 2006; Strauss et al., 2006). In the Ugljevik section, the late Badenian sea-level fall is well expressed and we have indications for erosion at the B/S boundary as well. Yet, a direct contact of the topmost Badenian and the earliest Sarmatian benthic zones, low relief erosive surface and, except for the transgressive lag, a continuation of laminated marly facies, implies that the potential erosion at the B/S boundary in Ugljevik represents only a short hiatus. Another hiatus is presumably present within the Sarmatian interval below the start of oolite deposition marked by reddish oxidized variegated claystone pointing to an emersion surface (top Unit 12a). Oolites in the Central Paratethys are restricted to the late Sarmatian, where they reflect a short warming phase and installation of hypersaline conditions (Harzhauser and Piller, 2007).

6. Conclusions

Ugljevik is a reference section for the Badenian (middle Miocene) marine paleoenvironmental evolution of the southern part of the Central Paratethys and Pannonian Basin. The continuous succession correlates with the late Langhian and early Serravallian interval, coinciding with the MMCT global cooling event and the environmental perturbations leading to the Badenian Salinity Crisis in the eastern Central Paratethys. The complete lack of evaporites in the section suggests a different paleoenvironmental evolution than in the eastern Central Paratethys. Faunal assemblages indicate an uninterrupted connectivity between the western Central Paratethys and the Mediterranean during the BSC.

The whole Ugljevik section is bio-magnetostratigraphically dated between ~14.2 and 12.5 Ma (Chrons C5ACr to C5Ar.1r). The present age model relates the late Badenian (early Serravallian) transgression-regression sequence to a single 1.2-My-obliquity cycle, with minimum values of both the 400- and 100-kyr cycle eccentricity cycle roughly correlating with the sea-level low stands. The calcareous nannoplankton bio-events in the section correspond well to those dated in the Mediterranean, pointing to well established marine connection at least until the NN5/NN6 boundary.

The age of the Badenian marine flooding (~14.2 Ma) in Ugljevik is slightly delayed compared to many other Pannonian sub-basins, suggesting a strong relation to tectonically controlled subsidence. The end of the MMCT and the Mi-3b sea level drop are expressed by a lowstand of about 150 m-magnitude, associated with an abrupt shift to carbonate deposition (~13.8–13.7 Ma), followed by a gradual base level rise of ~200 m. Presumably, the Pannonian Basin was semi-separated from the eastern Central Paratethys by a sill, restricting the long-distance influence of the Eastern Paratethys brackish water spillover that presumably triggered the BSC evaporite deposition in the Carpathian Foredeep. Water was nevertheless stratified to a certain degree in the Southern Pannonian Basin, as marked by blooms of planktonic gastropods and diatoms in the lower part of the late Badenian interval overlapping with the timing of the BSC. The high primary production stops with the decreasing volcanism and the sea level fall clearly noted between ~13.5 and 13.35 Ma by the beginning of the *U. jafari* nannoplankton assemblage.

An irregular omission surface at the B/S boundary with transgressive lag, bearing lithified mud clasts and silicified or coalified trunks, and reworked Badenian mollusks at the base of the Sarmatian, point to some erosion. The presented age model (option 1) places the B/S boundary and corresponding major Paratethys paleoenvironmental and faunal turnover event (BSEE) at ~12.6 Ma. The endemic benthic fauna of the Sarmatian interval points to a restriction of the connection to the Mediterranean and increased faunal exchange with the Eastern Paratethys, which might have been enhanced by a relative sea level lowstand or tectonic processes restricting the connection between the Pannonian Basin and the Mediterranean.

Acknowledgments

Our sincere thanks go to the authorities of RiTE Ugljevik for a permit to work in the mine area. We are highly indebted to Svetlana Renovica and her mining geologist team for hospitality and help with the fieldwork. Finally, we are grateful to Hazim Hrvatović (Federal Geological Survey Sarajevo) for his continued support. This research was financially supported by the Netherlands Organization for Scientific Research (NWO) via VICI project 865.10.011, and by the Netherlands Research Centre for Integrated Solid Earth Sciences (ISES).

Appendix A. Supplementary data

Supplementary data to this article can be found online at https://doi.org/10.1016/j.gloplacha.2018.10.010.

References

Abdul Aziz, H., Di Stefano, A., Foresi, L.M., Hilgen, F.J., Iaccarino, S.M., Kuiper, K.F., Lirer, F., Salvatorini, G., Turco, E., 2008. Integrated stratigraphy and $^{40}Ar/^{39}Ar$ chronology of early Middle Miocene sediments from DSDP Leg 42A, Site 372 (Western Mediterranean). Palaeogeogr. Palaeoclimatol. Palaeoecol. 257, 123–138.

Abels, H.A., Hilgen, F.J., Krijgsman, W., Kruk, R.W., Raffi, I., Turco, E., Zachariasse, W.J., 2005. Long-period orbital control on middle Miocene global cooling: integrated stratigraphy and astronomical tuning of the Blue Clay Formation on Malta. Paleoceanography 20https://doi.org/10.1029/2004PA001129. PA4012.

Aubry, M.P., 1992. Late Paleogene calcareous nannoplankton evolution: a tale of climatic deterioration. In: Prothero, D.R., Berggren, W.A. (Eds.), Eocene-Oligocene Climatic and Biotic Evolution. Princeton University Press, New Jersey, pp. 272–309.

Auer, G., Piller, W.E., Harzhauser, M., 2015. Two distinct decadal and centennial cyclicities forced marine upwelling intensity and precipitation during the late early Miocene in Central Europe. Clim. Past 11, 283–303.

Babel, M., 2004. Badenian evaporite basin of the northern Carpathian Foredeep as a drawdown Salina basin. Acta Geol. Pol. 54 (3), 313–337.

Backman, J., Raffi, I., 1997. Calibration of Miocene nannofossil events to orbitally tuned cyclostratigraphies from Ceara Rise. In: Shackleton, N.J., Curry, W.B., Richter, C., Bralower, T.J. (Eds.), Proceedings of the Ocean Drilling Program, 154 Scientific Results. Ocean Drilling Program, pp. 83–99.

Balázs, A., Matenco, L., Magyar, I., Horváth, F., Cloetingh, S., 2016. The link between tectonics and sedimentation in back-arc basins: new genetic constraints from the analysis of the Pannonian Basin. Tectonics 35, 1526–1559.

Báldi, K., 2006. Paleoceanography and climate in the Badenian (Middle Miocene, 16.4 - 13.0 Ma) in the Central Paratethys based on foraminifer and stable isotope evidence. Int. J. Earth Sci. 95, 119–142.

Báldi, K., Velledits, F., Ćorić, S., Lemberkovics, V., Lőrincz, K., Shevelev, M., 2017. Discovery of the Badenian evaporites inside the Carpathian Arc: implications for global climate change and Paratethys salinity. Geol. Carpath. 68, 193–206.

Barnes, P.A.G., Hickman, C.S., 1999. Lucinid bivalves and marine angiosperms: a search for causal relationships. In: Walker, D.I., Wells, F.E. (Eds.), The Seagrass Flora and Fauna of Rottnest Isand, Western Australia, Western Australian Museum, Perth, pp. 215–238.

Bartol, M., 2009. Middle Miocene Calcareus Nannoplankton of NE Slovenia (Western Central Paratethys). Paleontološki inštitut Ivana Rakovca ZRC SAZU, Ljubljana. Vol. 136.

Bartol, M., Mikuž, V., Horvat, A., 2014. Palaeontological evidence of communication between the Central Paratethys and the Mediterranean in the late Badenian/early Serravalian. Palaeogeogr. Palaeoclimatol. Palaeoecol. 394, 144–157.
Beldean, C., Bercea, R., Filipescu, S., 2013. Sedimentology and biostratigraphy of the Early-Middle Miocene transition in NW Transylvanian Basin (Pâglişa and Dej sections). Stud. Univ. Babes-Bolyai Geol. 58, 57–70.
Bicchi, E., Ferrero, E., Gonera, G., 2003. Palaeoclimatic interpretation based on Middle Miocene planktonic Foraminifera: the Silesia Basin (Paratethys) and Monferrato (Tethys) records. Palaeogeogr. Palaeoclimatol. Palaeoecol. 196, 265–303.
Bojar, A.-V., Barbu, V., Wojtowicz, A., Bojar, H.-P., Halas, S., Duliu, O., 2018. Miocene Slănic Tuff, Eastern Carpathians, Romania, in the Context of Badenian Salinity Crisis. Geosciences 8, 73. https://doi.org/10.3390/geosciences8020073.
Bukowski, K., Czapowski, G., Karoli, S., Babel, M., 2007. Sedimentology and geochemistry of the Middle Miocene (Badenian) salt-bearing succession from East Slovakian Basin (Zbudza Formation). Geol. Soc. Lond. Spec. Publ. 285, 247–264. https://doi.org/10.1144/SP285.14.
Bukry, D., Douglas, R.G., Kling, S.A., Krasheninnikov, V., 1971. Planktonic microfossil biostratigraphy of the northwestern Pacific Ocean. Initial Rep. Deep Sea Drill. Proj. 6, 1253–1300.
Čičić, S., Jovanović, Č., 1987. Contribution to knowledge of geological structure, genesis, evolution and tectonics of Tuzla basin with emphasis to conditions of Jala and Solina watersheed (in Bosnian/Serbian/Croatian). Geol. Glasnik Sarajevo 30, 113–155.
Čičić, S., Mojićević, M., Jovanović, Č., Tokić, S., Dimitrov, P., 1990. Osnovna geološka karta SFR Jugoslavije 1:100.000, list Tuzla. Savezni geološki zavod, Beograd.
Čičić, S., Mojićević, M., Jovanović, Č., Tokić, S., Dimitrov, P., 1991. Osnovna geološka karta SFR Jugoslavije 1:100.000, Tumač za list Tuzla. Beograd: Savezni geološki zavod. pp. 1–73.
Ćorić, S., Hohenegger, J., 2008. Quantitative analyses of calcareous nannoplankton assemblages from the Baden-Sooss section (Middle Miocene of Vienna Basin, Austria). Geol. Carpath. 59, 447–460.
Ćorić, S., Rögl, F., 2004. Roggendorf-1 borehole, a keysection for lower Badenian transgressions and the stratigraphic position of the Grund Formation (Molasse Basin, Lower Austria). Geol. Carpathica 55, 165–178.
Ćorić, S., Vrabac, S., Ferhatbegović, Z., Đulović, I., 2007. Biostratigraphy of Middle Miocene sediments from the Tuzla Basin (North-eastern Bosnia) based on foraminifera and calcareous nannoplankton. Joannea Geol. Palaont. 9, 21–23.
Ćorić, S., Pavelić, D., Rögl, F., Mandic, O., Vrabac, S., 2009. Revised Middle Miocene datum for initial marine flooding of North Croatian Basins (Pannonian Basin System, Central Paratethys). Geol. Croatica 62, 31–43.
De Boer, B., Van De Wal, R.S.W., Bintanja, R., Lourens, L.J., Tuenter, E., 2010. Cenozoic global ice-volume and temperature simulations with 1-D ice-sheet models forced by benthic $d^{18}O$ records. Ann. Glaciol. 51, 23–33.
de Bruijn, H., Marković, Z., Wessels, W., 2013. Late Oligocene rodents from Banovići (Bosnia and Herzegovina). Palaeodiversity 6, 63–105.
de Leeuw, A., Bukowski, K., Krijgsman, W., Kuiper, K.F., 2010. Age of the Badenian salinity crisis; impact of Miocene climate variability on the circum-Mediterranean region. Geology 38, 715–718.
de Leeuw, A., Mandic, O., de Bruijn, H., Marković, Z., Reumer, J., Wessels, W., Šišić, E., Krijgsman, W., 2011. Magnetostratigraphy and small mammals of the late Oligocene Banovići basin in NE Bosnia and Herzegovina. Palaeogeogr. Palaeoclimatol. Palaeoecol. 310, 400–412.
de Leeuw, A., Tulbure, M., Kuiper, K.F., Melinte-Dobrinescu, M.C., Stoica, M., Krijgsman, W., 2018. New 40Ar/39Ar, magnetostratigraphic and biostratigraphic constraints on the termination of the Badenian Salinity Crisis: evidence for tectonic improvement of basin interconnectivity in Southern Europe. Glob. Planet. Change Accepted. https://doi.org/10.1016/j.cageo.2011.03.003.As.
Dominici, S., Danise, S., Benvenuti, M., 2018. Pliocene stratigraphic paleobiology in Tuscany and the fossil record of marine megafauna. Earth-Sci. Rev. 176, 277–310.
Flores, J.A., Sierro, F.J., Raffi, I., 1995. Evolution of the Calcareous Nannofossil Assemblage as a Response to the Paleoceanographic Changes in the Eastern Equatorial Pacific Ocean from 4 to 2 Ma (Leg 138, Sites 849 and 852). Proceedings of the Ocean Drilling Program, Scientific Results. 138. pp. 163–176.
Fodor, L., Csontos, L., Bada, G., Gyorfi, I., Benkovics, L., 1999. Tertiary tectonic evolution of the Pannonian Basin system and neighbouring orogens: a new synthesis of palaeostress data. Geol. Soc. Lond. Spec. Publ. 156, 295–334.
Galindo, L.A., Puillandre, N., Utge, J., Lozouet, P., Bouchet, P., 2016. The phylogeny and systematics of the Nassariidae revisited (Gastropoda, Buccinoidea). Mol. Phylogenet. Evol. 99, 337–353.
Gonera, M., Peryt, T.M., Durakiewicz, T., 2000. Biostratigraphical and palaeoenvironmental implications of isotopic studies (^{18}O, ^{13}C) of middle Miocene (Badenian) foraminifers in the Central Paratethys. Terra Nova 12, 231–238.
Grunert, P., Soliman, A., Harzhauser, M., Müllegger, S., Piller, W., Roetzel, R., Rögl, F., 2010. Upwelling conditions in the early Miocene Central Paratethys Sea. Geol. Carpath. 61, 12–145.
Handford, C.R., Loucks, R.C., 1993. Carbonate depositional sequences and systems tracts responses of carbonate platforms to Relative Sea-Level changes. AAPG Mem. 57, 3–41.
Haq, B.U., 1980. Biogeographic history of Miocene calcareous nannoplankton and paleoceanography of the Atlantic Ocean. Micropaleontology 26 (4), 414–443.
Harzhauser, M., Piller, W.E., 2004. Integrated stratigraphy of the Sarmatian (Upper Middle Miocene) in the western. Central Paratethys. Stratigr. 1, 65–86.
Harzhauser, M., Piller, W.E., 2007. Benchmark data of a changing sea — Palaeogeography, Palaeobiogeography and events in the Central Paratethys during the Miocene. Palaeogeogr. Palaeoclimatol. Palaeoecol. 253, 8–31.
Harzhauser, M., Grunert, P., Mandic, O., Lukeneder, P., García Gallardo, Á., Neubauer, T.A., Carnevale, G., Landau, B.M., Sauer, R., Strauss, P., 2018. Middle and late Badenian palaeoenvironments in the northern Vienna Basin and their potential link to the Badenian Salinity Crisis. Geol. Carpath. 69, 129–168.
Hilgen, F.J., Abels, H.A., Iaccarino, S., Krijgsman, W., Raffi, I., Sprovieri, R., 2009. The global stratotype section and point (GSSP) of the Serravallian stage (Middle Miocene). Episodes 32, 152–166.
Hilgen, F.J., Lourens, L.J., Van Dam, J.A., Ogg, J.G., 2012. The Neogene period. In: Gradstein, F.M., Schmitz, M.D., Ogg, G.M. (Eds.), The Geologic Time Scale 2012. Vol. 2. Elsevier, Amsterdam, pp. 923–978.
Hohenegger, J., Wagreich, M., 2012. Time calibration of sedimentary sections based on insolation cycles using combined cross-correlation: dating the gone Badenian stratotype (Middle Miocene, Paratethys, Vienna Basin, Austria) as an example. Int. J. Earth Sci. 101, 339–349.
Hohenegger, J., Rögl, F., Ćorić, S., Pervesler, P., Lirer, F., Roetzel, R., Scholger, R., Stingl, K., 2009. The Styrian basin: a key to the Middle Miocene (Badenian/Langhian) Central Paratethys transgressions. Austrian J. Earth Sci. 102.
Holbourn, A., Kuhnt, W., Schulz, M., Flores, J.A., Andersen, N., 2007. Orbitally-paced climate evolution during the middle Miocene "Monterey" carbon-isotope excursion. Earth Planet. Sci. Lett. 261, 534–550.
Holbourn, A., Kuhnt, W., Lyle, M., Schneider, L., Romero, O., Andersen, N., 2014. Middle Miocene climate cooling linked to intensification of eastern equatorial Pacific upwelling. Geology 42, 19–22.
Holbourn, A., Kuhnt, W., Kochhann, K.G.D., Andersen, N., Meier, S.K.J., 2015. Global perturbation of the carbon cycle at the onset of the Miocene Climatic Optimum. Geology 43 (2), 123–126.
Horváth, F., Musitz, B., Balázs, A., Végh, A., Uhrin, A., Nádor, A., Koroknai, B., Pap, N., Tóth, T., Wórum, G., 2015. Evolution of the Pannonian basin and its geothermal resources. Geothermics 53, 328–352.
Hrvatović, H., 2006. Geological Guidebook Through Bosnia and Herzegovina. Geological Survey of Bosnia and Herzegovina, Sarajevo.
Hüsing, S.K., Dekkers, M.J., Franke, C., Krijgsman, W., 2009. The Tortonian reference section at Monte dei Corvi (Italy): evidence for early remanence acquisition in greigite-bearing sediments. Geophys. J. Int. 179, 125–143.
Ilić, A., Neubauer, F., 2005. Tertiary to recent oblique convergence and wrenching of the Central Dinarides: constraints from a palaeostress study. Tectonophysics 410, 465–484.
John, C.M., Karner, G.D., Browning, E., Leckie, R.M., Mateo, Z., Carson, B., Lowery, C., 2011. Timing and magnitude of Miocene eustasy derived from the mixed siliciclastic-carbonate stratigraphic record of the northeastern Australian margin. Earth Planet. Sci. Lett. 304, 455–467.
Kirschvink, J.L., 1980. The least-squares line and plane and the analysis of palaeomagnetic data. Geophys. J. Int. 62, 699–718.
Kominz, M.A., Browning, J.V., Miller, K.G., Sugarman, P.J., Mizintseva, S., Scotese, C.R., 2008. Late cretaceous to Miocene Sea-level estimates from the New Jersey and Delaware coastal plain coreholes: an error analysis. Basin Res. 20, 211–226.
Kováč, M., Baráth, I., Harzhauser, M., Hlavatý, I., Hudáčková, N., 2004. Miocene depositional systems and sequence stratigraphy of the Vienna Basin Depositional systems and sequence stratigraphy. Courier Forschungsinstitut Senckenberg 246, 187–212.
Kováč, M., Andreyeva-Grigorovich, A., Bajraktarević, Z., Brzobohatý, R., Filipescu, S., Fodor, L., Harzhauser, M., Nagymarosy, A., Oszczypko, N., Pavelić, D., Rögl, F., Saftić, B., Sliva, U., Studencka, B., 2007. Badenian evolution of the Central Paratethys Sea: paleogeography, climate and eustatic sea-level changes. Geol. Carpath. 58, 579–606.
Kováč, M., Hudáčková, N., Halásová, E., Kováčová, M., Holcová, K., Oszczypko-Clowes, M., Báldi, K., Less, G., Nagymarosy, A., Ruman, A., Klučiar, T., Jamrich, M., 2017. The Central Paratethys palaeoceanography: a water circulation model based on microfossil proxies, climate, and changes of depositional environment. Acta Geol. Slovaca 9, 75–114.
Kováčová, P., Emmanuel, L., Hudáčková, N., Renard, M., 2008. Central Paratethys paleoenvironment during the Badenian (Middle Miocene): evidence from foraminifera and stable isotope (d13C and d18O) study in the Vienna Basin (Slovakia). Int. J. Earth Sci. 98, 1109–1127.
Krézsek, C., Bally, A.W., 2006. The Transylvanian Basin (Romania) and its relation to the Carpathian fold and thrust belt: insights in gravitational salt tectonics. Mar. Pet. Geol. 23, 405–442.
Krhovský, J., Adamova, J., Hladikova, J., Maslowska, H., 1992. Paleoenvironmental changes across the Eocene/Oligocene boundary in the Zdanice and Pouzdrany units (western Carpathians, Czechoslovakia): the long-term trend and orbitally forced changes in calcareous nannofossil assemblages. Knihovicka ZPN 14b, 105–187.
Krijgsman, W., Tauxe, L., 2004. Shallow bias in Mediterranean paleomagnetic directions caused by inclination error. Earth Planet. Sci. Lett. 222, 685–695.
Kruiver, P.P., Dekkers, M.J., Heslop, D., 2001. Quantification of magnetic coercivity components by the analysis of acquisition curves of isothermal remanent magnetisation. Earth Planet. Sci. Lett. 189, 269–276.
Kruiver, P.P., Langereis, C.G., Dekkers, M.J., Krijgsman, W., 2003. Rock-magnetic properties of multicomponent natural remanent magnetization in alluvial red beds (NE Spain). Geophys. J. Int. 153, 317–332.
Laskar, J., Robutel, P., Joutel, F., Gastineau, M., Correia, A.C.M., Levrard, B., 2004. A long-term numerical solution for the insolation quantities of the Earth. Astron. Astrophys. 428, 261–285.
Lukacs, R., Harangi, S., Guillong, M., Bachmann, O., Fodor, L., Buret, Y., Dunkl, I., Sliwinski, J., van Quadt, A., Peytcheva, I., Zimmerer, M., 2018. Early to Mid-Miocene syn-extensional massive silicic volcanism in the Pannonian Basin (East-Central Europe): eruption chronology, correlation potential and geodynamic implications. Earth Sci. Rev. 179, 1–19.
Malez, M., Thenius, E., 1985. Über das Vorkommen von Amynodonten (Rhinocerotoidea,

Mammalia) im Oligo-Miozän von Bosnien (Jugoslawien). Paleaontologia Jugoslavica 34, 1–26.
Mandic, O., 2004. Pectinid bivalves from the Grund Formation (lower Badenian, Middle Miocene, Alpine-Carpathian Foredeep) – taxonomic revision and stratigraphic significance. Geol. Carpath. 55, 129–146.
Mandic, O., Harzhauser, M., 2003. Molluscs from the Badenian (Middle Miocene) of the Gaindorf Formation (Alpine Molasse Basin, NE Austria). Ann. Naturhist. Museums Wien 104, 85–127.
Mandic, O., Harzhauser, M., Roetzel, R., Tibuleac, P., 2008. Benthic mass-mortality events on a Middle Miocene incised-valley tidal-flat (North Alpine Foredeep Basin). Facies 54, 343–359.
Mandic, O., de Leeuw, A., Bulić, J., Kuiper, K.F., Krijgsman, W., Jurišić-Polšak, Z., 2012. Paleogeographic evolution of the Southern Pannonian Basin: $^{40}Ar/^{39}Ar$ age constraints on the Miocene continental series of Northern Croatia. Int. J. Earth Sci. 101, 1033–1046.
Martini, E., 1971. Standard tertiary and quaternary calcareous nannoplankton zonation. In: Farinacci, A. (Ed.), Proceedings of the Second Planktonic Conference, Roma 1970. Vol. 2. pp. 739–785 Rome: Edizioni Tecnoscienza.
Matenco, L., Radivojević, D., 2012. On the formation and evolution of the Pannonian Basin: constraints derived from the structure of the junction area between the Carpathians and Dinarides. Tectonics 31, 1944–9194.
McFadden, P.L., McElhinny, M.W., 1988. The combined analysis of remagnetization circles and direct observations in palaeomagnetism. Earth Planet. Sci. Lett. 87, 161–172.
Mojsilović, S., Filipović, I., Rodin, M., Baklaić, D., Đoković, I., Jovanović, Č., Živanović, D., Eremija, M., Cvetković, B., 1975. Osnovna geološka karta SFRJ, Zvornik, 1:100000. Beograd.
Mourik, A.A., Abels, H.A., Hilgen, F.J., Di Stefano, A., Zachariasse, W.J., 2011. Improved astronomical age constraints for the middle Miocene climate transition based on high-resolution stable isotope records from the Central Mediterranean Maltese Islands. Paleoceanography 26, 1–14.
Mullender, T.A.T., Frederichs, T., Hilgenfeldt, C., de Groot, L.V., Fabian, K., Dekkers, M.J., 2016. Automated paleomagnetic and rock magnetic data acquisition with an in-line horizontal “2G” system. Geochem. Geophys. Geosyst. 17, 3546–3559.
Murray, J.W., 1991. Ecology and paleoecology of Benthic foraminifera. Longman Sci. Tech, Harlow, Essex.
Okada, H., McIntyre, A., 1979. Seasonal distribution of the modern Coccolithophores in the western North Atlantic Ocean. Mar. Biol. 54, 319–328.
Palcu, D.V., Tulbure, M., Bartol, M., Kouwenhoven, T.J., Krijgsman, W., 2015. The Badenian – Sarmatian extinction event in the Carpathian foredeep basin of Romania: paleogeographic changes in the Paratethys domain. Glob. Planet. Chang. 133, 346–358.
Palcu, D.V., Golovina, L.A., Vernyhorova, Y.V., Popov, S.V., Krijgsman, W., 2017. Middle Miocene paleoenvironmental crises in Central Eurasia caused by changes in marine gateway configuration. Glob. Planet. Chang. 158, 57–71.
Papp, A., Cicha, I., Senes, J., Steininger, F., 1978. M4, Badenien (Moravien, Wielicien, Kosovien). Chronostratigraphie Und Neostratotypen, Miozän der Zentralen Paratethys. 6. pp. 1–594.
Paulissen, W., Luthi, S., Grunert, P., Ćorić, S., Harzhauser, M., 2011. Integrated high-resolution stratigraphy of a middle to late Miocene sedimentary sequence in the central part of the Vienna Basin. Geol. Carpath. 62, 155–169.
Pavelić, D., Kovačić, M., 2018. Sedimentology and stratigraphy of the Neogene rift-type North Croatian Basin (Pannonian Basin System, Croatia): a review. Mar. Pet. Geol. 91, 455–469.
Perch-Nielsen, K., 1985. Cenozoic calcareous nannofossils. In: Bolli, H.M., Saunders, J.B., Perch-Nielsen, K. (Eds.), Plankton Stratigraphy1. Cambridge University Press, Cambridge, pp. 427–554.
Peryt, T.M., 2006. The beginning, development and termination of the Middle Miocene Badenian salinity crisis in Central Paratethys. Sediment. Geol. 188–189, 379–396.
Peryt, D., 2013a. Foraminiferal record of the Middle Miocene climate transition prior to the Badenian salinity crisis in the Polish Carpathian Foredeep Basin (Central Paratethys). Geol. Q 57, 141–164.
Peryt, T.M., 2013b. Palaeogeographical zonation of gypsum facies: middle Miocene Badenian of Central Paratethys (Carpathian Foredeep in Europe). J. Palaeogeogr. 2 (3), 225–237.
Peryt, D., Peryt, T.M., 2009. Environmental changes in the declining Middle Miocene Badenian evaporite basin of the Ukrainian Carpathian Foredeep (Kudryntsi section). Geol. Carpath. 60, 505–517.
Peryt, D., Gedl, P., Peryt, T.M., 2014. Foraminiferal and palynological re cords of the late Badenian (Middle Miocene) transgression in Podolia (Shchyrets near Lviv, western Ukraine). Geol. Q 58, 465–483.
Pezelj, Đ., Mandic, O., Ćorić, S., 2013. Paleoenvironmental dynamics in the southern Pannonian Basin during initial Middle Miocene marine flooding. Geol. Carpath. 64, 81–100.
Pezelj, Đ., Sremac, J., Bermanec, V., 2016. Shallow-water benthic foraminiferal assemblages and their responce to the palaeoenvironmental changes - example from the Middle Miocene of Medvednica Mt. (Croatia, Central Paratethys). Geol. Carpath. 67, 329–345.
Piller, W.E., Harzhauser, M., 2005. The myth of the brackish Sarmatian Sea. Terra Nova 17, 450–455.
Popov, S.V., Rögl, F., Rozanov, A.Y., Steininger, F.F., Shcherba, I.G., Kovac, M., 2004. Lithological-paleogeographic maps of Paratethys. Courier Forschungsinstitut Senckenberg 250, 1–46.
Poppe, G.T., Goto, Y., 1993. Scaphopoda, Bivalvia, Cephalopoda. In: Poppe, G.T., Goto, Y. (Eds.), European Seashells. Verlag Christa Hemmen, Wiesbaden.
Rögl, F., 1998. Palaeogeographic considerations for Mediterranean and Paratethys Seaways (Oligocene to Miocene). In: Ann. des Naturhistorischen Museums Wien 99A, pp. 279–310.
Rupp, C., Hohenegger, J., 2008. Paleoecology of planktonic foraminifera from the Baden-Sooss section (Middle Miocene, Badenian, Vienna Basin, Austria). Geol. Carpath. 59, 425–445.
Rybár, S., Kováč, M., Šarinová, K., Halásová, E., Hudačková, N., Šujan, M., Kováčová, M., Ruman, A., Klučiar, T., 2016. Neogene changes in palaeogeography, palaeoenvironment and the provenance of sediment in the Northern Danube Basin Neogene changes in palaeogeography, palaeoenvironment and the provenance of sediment in the Northern Danube Basin. Bull. Geosci. 91, 367–398. https://doi.org/10.3140/bull.geosci.1571.
Sant, K., Palcu, D., Mandic, O., Krijgsman, W., 2017. Changing seas in the Early–Middle Miocene of Central Europe: a Mediterranean approach to Paratethyan stratigraphy. Terra Nova 29, 273–281.
Sant, K., Mandic, O., de Leeuw, A., Krijgsman, W., 2018a. Paleomagnetic dataset of the marine Badenian reference section Ugljevik in Bosnia-Herzegovina (Middle Miocene, Pannonian basin, Central Paratethys). GFZ Data Serv. https://doi.org/10.5880/fidgeo.2018.014. https://pmd.gfz-potsdam.de/panmetawork.
Sant, K., Mandic, O., Rundić, L.J., Kuiper, K.F., Krijgsman, W., 2018b. Age and evolution of the Serbian Lake System: integrated results from Middle Miocene Lake Popovac. Newsl. Stratigr. 51, 117–143.
Schlager, W., 2005. Carbonate sedimentology and sequence stratigraphy. SEPM Concept. Sedimentol. Paleontol. 8, 1–200.
Schmid, Bernoulli, D., Fügenschuh, B., Matenco, L., Schefer, S., Schuster, R., Tischler, M., Ustaszewski, K., 2008. The Alpine-Carpathian-Dinaridic orogenic system: correlation and evolution of tectonic units. Swiss J. Geosci. 101, 139–183.
Schreilechner, M.G., Sachsenhofer, R.F., 2007. High resolution sequence stratigraphy in the eastern styrian basin (Miocene, Austria). Austrian J. Earth Sci. 100, 164–184.
Selmeczi, I., Lantos, M., Bohn-Havas, M., Nagymarosy, A., Szegő, É., 2012. Correlation of bio- and magnetostratigraphy of Badenian sequences from western and northern Hungary. Geol. Carpath. 63, 219–232.
Shevenell, A.E., Kennett, J.P., Lea, D.W., 2004. Middle miocene southern ocean cooling and antarctic cryosphere expansion. Science 205, 1766–1770.
Śliwiński, M., Bábel, M., Nejbert, K., Olszewska-Nejbert, D., Gásiewicz, A., Schreiber, B.C., Benowitz, J.A., Layer, P., 2012. Badenian-Sarmatian chronostratigraphy in the Polish Carpathian Foredeep. Palaeogeogr. Palaeoclimatol. Palaeoecol. 326–328, 12–29.
Spezzaferri, S., Coric, S., Stingl, K., 2009. Palaeoenvironmental reconstruction of the Karpatian – Badenian (late Burdigalian – early Langhian) transition in the Central Paratethys. A case study from the Wagna Section (Austria). Acta Geol. Pol. 59, 523–544.
Stojadinović, U., Matenco, L., Andriessen, P.A.M., Toljić, M., Foeken, J.P.T., 2013. The balance between orogenic building and subsequent extension during the Tertiary evolution of the NE Dinarides: constraints from low-temperature thermochronology. Glob. Planet. Chang. 103, 19–38.
Strauss, P., Harzhauser, M., Hinsch, R., Wagreich, M., 2006. Sequence stratigraphy in a classic pull-apart basin (Neogene, Vienna Basin). A 3D seismic based integrated approach. Geol. Carpath. 57, 185–197.
Tallmark, B., 1980. Population dynamics of Nassarius reticulatus (Gastropoda, Prosobranchia) in Gullmar Fjord, Sweden. Mar. Ecol. Prog. Ser. 3, 51–62.
Tari, V., Pamić, J., 1998. Geodynamic evolution of the northern Dinarides and the southern part of the Pannonian Basin. Tectonophysics 297, 269–281.
Tauxe, L., Kent, D.V., 2004. A Simplified Statistical Model for the Geomagnetic Field and the Detection of Shallow Bias in Paleomagnetic Inclinations: Was the Ancient Magnetic Field Dipolar?, in: Timescales of the Paleomagnetic. American Geophysical Union, pp. 101–115.
ter Borgh, M., Vasiliev, I., Stoica, M., Knežević, S., Matenco, L., Krijgsman, W., Rundić, L., Cloetingh, S., 2013. The isolation of the Pannonian basin (Central Paratethys): new constraints from magnetostratigraphy and biostratigraphy. Glob. Planet. Chang. 103, 99–118.
Torsvik, T.H., Van der Voo, R., Preeden, U., Mac Niocaill, C., Steinberger, B., Doubrovine, P.V., van Hinsbergen, D.J.J., Domeier, M., Gaina, C., Tohver, E., Meert, J.G., McCausland, P.J.a., Cocks, L.R.M., 2012. Phanerozoic polar wander, palaeogeography and dynamics. Earth-Sci. Rev. 114, 325–368.
Túnyi, I., Vass, D., Karoli, S., Janocko, J., Halásová, E., Zlínská, A., Belácek, B., 2005. Magnetostratigraphy of Badenian evaporite deposits (East Slovak Basin). Geol. Carpath. 56, 273–284.
Ustaszewski, K., Schmid, S.M., Fügenschuh, B., Tischler, M., Kissling, E., Spakman, W., 2008. A map-view restoration of the alpine-carpathian-dinaridic system for the early miocene. Swiss J. Geosci. 101, 273–294.
Ustaszewski, K., Herak, M., Tomljenović, B., Herak, D., Matej, S., 2014. Neotectonics of the Dinarides-Pannonian Basin transition and possible earthquake sources in the Banja Luka epicentral area. J. Geodyn. 82, 52–68.
Vandamme, D., 1994. A new method to determine paleosecular variation. Phys. Earth Planet. Inter. 85, 131–142.
Vrabac, S., Ćorić, S., Đulović, I., Ječmenica, Z., 2015. Diskordancija između badena i sarmata u profilu Spasine kod Ugljevika, in: Proceedings, congress of geologists in Bosnia and Herzegovina, Tuzla, (Geological society of Bosnia and Herzegovina). pp. 1–25.
Wade, B.S., Bown, P.R., 2006. Calcareous nannofossils in extreme environments: the messinian salinity crisis, polemi basin, cyprus. Palaeogeogr. Palaeoclimatol. Palaeoecol. 233, 271–286.
Wessels, W., Markovic, Z., de Bruijn, H., Daxner-Hock, G., Mandic, O., Sisic, E., 2008. Paleogeography of late oligocene to miocene rodent assemblages from the western Dinaride-Anatolian Land. Geophys. Res. Abstr. 10 (EGU2008-A-07018).
Winter, A., Jordan, R., Roth, P., 1994. Biogeography of living Coccolithophores in ocean

waters. In: Winter, A., Siesser, W. (Eds.), Coccolithophores. Cambridge University Press, Cambridge, pp. 13–37.
Wisshak, M., López Correa, M., Gofas, S., Salas, C., Taviani, M., Jakobsen, J., Freiwald, A., 2009. Shell architecture, element composition, and stable isotope signature of the giant deep-sea oyster *Neopycnodonte zibrowii* sp. n. from the NE Atlantic. Deep. Res. I 66, 374–407.
Zachos, J., Pagani, M., Sloan, L., Thomas, E., Billups, K., 2001. Trends, rhythms, and aberrations in global climate 65 Ma to present. Science 292, 686–693.
Zijderveld, J.D.A., 1967. Demagnetization of rocks: analysis of results. In: Collinson, D.W., Creer, K.M., Runcom, S.K. (Eds.), Methods in Paleomagnetism. Elsevier, Amsterdam, pp. 254–286.